Marine Geology 425 (2020) 106190

Contents lists available at ScienceDirect

Marine Geology

journal homepage: www.elsevier.com/locate/margo

Linkage between turbulent kinetic energy, waves and suspended sediment concentrations in the nearshore zone

Wenhong Pang[a], Zhijun Dai[a,b,*], Binbin Ma[a], Jie Wang[a], Hu Huang[c], Shushi Li[c]

[a] State Key Laboratory of Estuarine and Coastal Research, East China Normal University, Shanghai 200062, China
[b] Laboratory for Marine Geology, Qingdao National Laboratory for Marine Science and Technology, Qingdao 266061, China
[c] Key Laboratory of Coastal Science and Engineering, Beibu Gulf, Guangxi, Beibu Gulf University, Qinzhou 535011, Guangxi, China

ARTICLE INFO

Editor: Edward Anthony

Keywords:
Turbulent kinetic energy
Suspended sediment concentration
Waves
Nearshore zone

ABSTRACT

Knowledge about the tradeoffs among turbulent kinetic energy (TKE), waves, and suspended sediment concentrations (SSCs) in the nearshore zone is relevant for understanding beach morphodynamics at different temporal and spatial scales. A field measurement lasting for nearly three tidal cycles was conducted to holistically discern couplings between TKE, waves and SSCs, with further evaluation of the relative significance of TKE and waves on SSCs under various wave conditions over a meso-macro tidal beach, Yintan, to the north of Beibu Gulf, China. The results showed a dramatic increase in wave groupiness intensity from the shoaling wave condition to the breaking wave condition and a clear decrease further into the surf bore condition. The near-bed TKEs under the surf bore condition were an order of magnitude larger than those under the breaking and shoaling wave conditions at the measurement position. The averaged SSCs in the near-bed (approximately 10 cm) under the surf bore condition were 1.5 and 4.5 times larger than those under breaking and shoaling wave conditions, respectively. The variations in relative wave height were a decisive indicator for the differences in TKE intensities among different wave conditions, while the occurrence of peak TKEs at the wave front within the intrawave cycle was associated with flow acceleration regardless of wave conditions. Mean SSCs were well correlated with waves in terms of both incident wave scale and wave group scale, which was limited to the shoaling wave condition, and the occurrence of near-bed intrawave peak SSCs was always related to the offshore wave phase. Further, TKE contributed more effectively to sediment suspension at the wave group scale than at the incident wave scale, especially under broken wave condition. Among the hydrodynamic factors, TKE played the most important role in the variations in SSCs for all wave conditions. Flow acceleration served as the second most important factor under the broken wave condition, while wave group, single wave and advection were equivalent and less important factors for SSCs.

1. Introduction

The coastal hydrodynamic conditions and corresponding near-bed suspended sediment concentrations (SSCs) are significant in controlling the vast majority of beach sand motions and the subsequent beach morphology evolution (Jaffe et al., 1984; Dai et al., 2010; Bolaños et al., 2012; Leonardi et al., 2015; Hu et al., 2018). As important components of coastal hydrodynamics, the turbulence produced by waves and the wave orbital motions determine the amount of suspended sediment in the water column and the direction and magnitude of near-bed suspended sediment transport (SST) in the nearshore zone (Soulsby and Humphery, 1990; Aagaard and Greenwood, 1995; Aagaard and Hughes, 2010; Brinkkemper et al., 2017). The coupling between turbulent kinetic energy (TKE), waves and SSC may act as a key mechanism in controlling the beach morphodynamic process (Scott et al., 2009; Hu et al., 2015; Leclaire and Ting, 2017). However, little information is available regarding the tradeoffs among waves, turbulence and SSC over the nearshore zone.

It has been confirmed that waves, including incident waves, infragravity waves and wave groups, play important roles in both sediment mobilization and the resulting suspended sediment transport (SST) (Conley and Beach, 2003; Gonzalez-Rodriguez and Madsen, 2007; Fagherazzi et al., 2010; Alsina et al., 2018). For incident waves that propagate shoreward, sediment grains are usually stirred up into the water column at both the wave trough and crest, which led to the occurrence of peak SSCs during each half wave cycle (Kularatne and Pattiaratchi, 2008; Murray et al., 2011; Aagaard and Jensen, 2013). Researchers have attributed the phenomenon to higher velocity-

* Corresponding author at: State Key Laboratory of Estuarine and Coastal Research, East China Normal University, Shanghai 200062, China.
E-mail address: zjdai@sklec.ecnu.edu.cn (Z. Dai).

https://doi.org/10.1016/j.margeo.2020.106190
Received 11 October 2019; Received in revised form 21 March 2020; Accepted 25 March 2020
Available online 11 April 2020

induced bed shear stress during the onshore phase of the wave cycle and to the influence of vortex ripples. In general, different wave heights were mainly responsible for the variations in average SSCs in the water column due to its primary contribution to the mechanism of sediment suspension compared to other factors, such as bed configuration and mean current (Aagaard and Greenwood, 1995; Puleo et al., 2003; Conley and Beach, 2003; Miles and Thorpe, 2015). However, the near-bed SSCs do not vary linearly following wave heights. It was suggested that very near-bed SSCs increased gradually as the wave energy intensified persistently, while SSCs at higher elevations declined once the wave energy was strong enough to transform the bedforms from vortex ripples to post-vortex ripples and a planar seabed (Ribberink and Al-Salem, 1995). In fact, the precise intra-ave distributions of SSCs are determined by the coupling between wave height, wave period, sediment grain size, ripple morphology and breaking wave-induced turbulence, which need to be comprehensively studied in future work (i.e., Osborne and Greenwood, 1993; Grasmeijer and Kleinhans, 2004; Christensen et al., 2019).

Meanwhile, wave groups which consist of a succession of incident waves whose heights are not all of equal length (Longuet-Higgins, 1984), could contribute more SSCs than a single incident wave by generating surficial SSCs of more than three times than that under a single incident wave at the same elevation (Murray et al., 2012), as well as increasing vertical suspended sediment fluxes (Williams et al., 2002). The wave groups with increasing wave heights followed by decreasing wave heights are more capable than those with constant wave heights of pumping and entraining the sediment from the seabed (Villard et al., 2000; Vincent and Hanes, 2002; Murray et al., 2012). Moreover, the peak SSC occurred at the time where wave groups began to weaken following the largest incident wave (Villard et al., 2000). In addition, sediment suspension can be significantly affected by infragravity wave when infragravity wave orbital velocity increased distinctly and even equaled or exceeded the incident wave orbital velocity, especially within the surf zone under energetic wave conditions (Aagaard and Greenwood, 1995). To be specific, the relative contribution of infragravity wave to sediment suspension is associated with beach slope as well as the ratio of infragravity wave height to incident wave height (De Bakker et al., 2016). For instance, the more gentle beach slope is, the more incident wave energy is dissipated along with the release of infragravity wave after wave breaking (Longuet-Higgins and Stewart, 1964; Symonds et al., 1982; Baldock and Swan, 1996), which leads to higher infragravity wave-induced orbital velocity than incident wave (Bertin et al., 2018). However, the relative importance of incident waves, infragravity wave and wave group on sediment suspension and the subsequent SSCs have been less evaluated synchronously.

Furthermore, it has been proven that waves also greatly contribute to TKE by means of both bed and surface-generated turbulence induced by waves (van der Werf et al., 2007; Brinkkemper et al., 2016). Under shoaling wave condition, friction between wave orbital motion and the seabed at the wave troughs and wave crests are the main sources of turbulence generation (Nielsen et al., 2002; Christensen et al., 2019). High TKEs occur at the moment where the wave phase converted between onshore and offshore phases, which is associated with the ejection of turbulent eddies over a rippled bedform (Aagaard and Jensen, 2013). Under the breaking zone where breaking waves conditions prevail, turbulent eddies are generated by waves striking the water surface (Nadaoka et al., 1989; Stansby and Feng, 2005) and TKEs are primarily determined by the shape of the incident wave spectrum (Ting, 2002). Further into the surf bore conditions, the generation of turbulence is associated with breaking wave-induced surf bores which is dominated by incident wave period and wave height, and it displays more vertical mixing downward the seabed compared with that under the breaking wave condition (Ting, 2002). However, peak TKEs exist under either the onshore phase or offshore phase for both the spilling breaker and plunging breaker, depending on the TKE dissipation rate along the path of turbulent eddies downwards of the seabed (Nielsen, 2006; Christensen et al., 2019). Therefore, further studies are needed to predict TKE variations with a wave-related indicator under various wave conditions.

Turbulent motions are a critical factor for sediment suspension and increasing SSCs (Heathershaw, 1974; Foster et al., 1994; Yoon and Cox, 2012) by enhancing the current-induced bed shear stress (LeClaire and Ting, 2017), which has been confirmed in both field observations (Aagaard and Hughes, 2010; Kassem et al., 2015) and sediment transport models (Butt et al., 2004; Aagaard and Hughes, 2006; Kobayashi et al., 2008). The higher the TKE intensity is, the more SSCs are produced in the water, which is consistent with observations that the SSCs and TKEs are significantly larger under the breaking wave and surf bore conditions than that under the nonbreaking wave condition (Hansen and Svendsen, 1984; Yu et al., 1993; Beach and Sternberg, 1996). Moreover, turbulent eddies mix suspended sediment vertically upward to higher elevations above the seabed and lead to the phase lag of peak SSCs between the near-bed area and dozens of centimeters above the seabed (Murray et al., 2012). Further, studies have related the sediment suspension to the second peak in surface elevation (a change in the rate of water level decrease) and the 'burst' event of TKE under the shoaling wave condition (Kularatne and Pattiaratchi, 2008), while sediment suspension in the surf condition coincides well with a negative peak of infragravity wave-induced horizontal velocity and incident bores (Alsina and Cáceres, 2011). Moreover, it has been demonstrated by LeClaire and Ting (2017) that the generated high SSCs tend to be explained well by the TKEs contained within the counter-rotating vortices and that other sources of TKEs may not contribute to sediment suspension. Thus, more studies need to be conducted to understand the role of TKEs in the mechanism of sediment suspension.

Although much attention has been paid to the influence of wave orbital motions on TKEs and sediment motions as well as to the relationship between turbulence and intermittent sediment suspension (Ting, 2002; Kularatne and Pattiaratchi, 2008; Fagherazzi et al., 2010; Yoon and Cox, 2012), few studies have focused on the interrelation among TKE, waves and SSCs at different wave scales and relative importance of various hydrodynamic forces on the variations of SSCs in the nearshore zone. Therefore, the purposes of this paper are 1) to detect the interrelation among waves, TKE and SSCs at different wave scales and 2) to evaluate the relative importance of TKE and waves on SSCs. The results of this work may be of great significance in the assessment of coastal zone responses to changing oceanic forces.

2. Methodology

2.1. Study settings

A comprehensive field observation was conducted at Yintan Beach (Fig. 1), Beihai City, China, from 28th May 2016 to 31st May 2016. The beach is defined as a meso-macro tidal beach with a mean spring tidal range of 3.6 m, and experiences diurnal tidal conditions during middle and spring tides, whereas a semidiurnal tide prevails during neap tides (Pang et al., 2019). The depth-averaged values of flood and ebb tidal currents during the spring tide are 0.13 m/s and 0.31 m/s, respectively (Huang et al., 2011). The mean wave height in this region is approximately 0.5 m and changes significantly along the seasons (Zhou et al., 2015). In addition, the wave direction is northward in winter and southwest in summer due to the impacts of the southwest monsoon (Huang et al., 2011).

Multiple sandbar systems develop both in intertidal and subtidal zones over the nearshore area (Ge et al., 2017). An obvious and straight sandbar exists on the upper beach with an angle of 28° between the sandbar and latitude line (Ge et al., 2017; Pang et al., 2019). The sediments here mainly consist of unconsolidated quartz sands, and the median grain size varies from 0.14 mm to 0.20 mm across the intertidal region (Huang et al., 2011; Ge et al., 2017), which leads to an average slope of 0.02 over Yintan Beach.

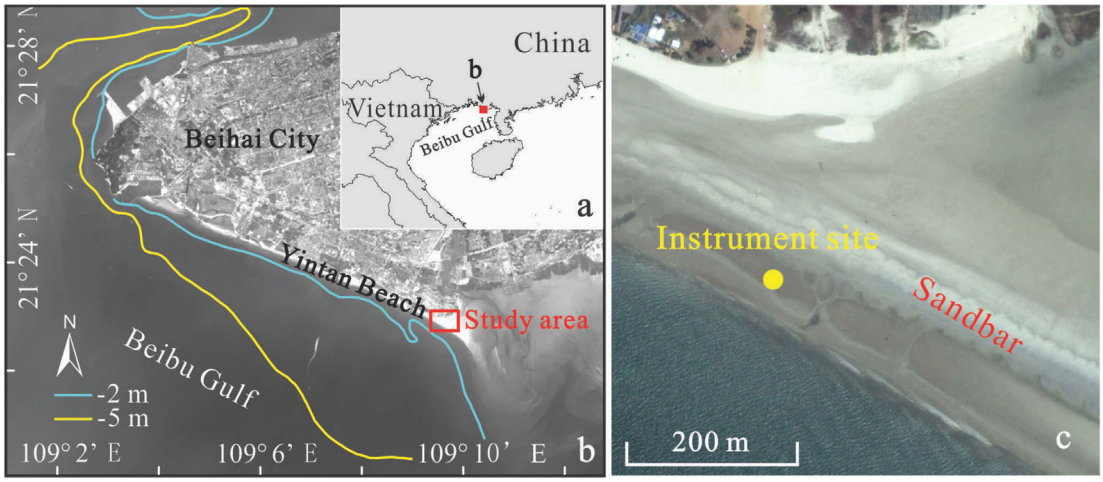

Fig. 1. Study area with (a) location of Beibu Gulf, (b) location of Yintan Beach and (c) instrument site.

2.2. Instrument deployment

The field measurement was conducted in the nearshore area of Yintan Beach (Fig. 2a), which lasted over three tidal cycles between 28th May 2016 and 31st May 2016. During the observation, a rig (Fig. 2b) was equipped with a 6 MHz Nortek acoustic Doppler velocimeter (ADV) to record the high-resolution 3D flow velocity (u, v and w) in three directions; an Argus surface meter (ASM-IV) was used to measure the vertical profile of water turbidity (transformed to SSC, $R^2 = 0.99$, $P < 0.001$, Fig. S1) (full details for the calibration of ASM-IV sensors are provided in the Supporting Information, Text S1, Fig. S1); an optical backscatter sensor (OBS-3A) was used to measure water depth (h), and a tide and wave recorder (RBR-2050) was used to obtain the water surface elevation (η) and significant wave height (H_s).

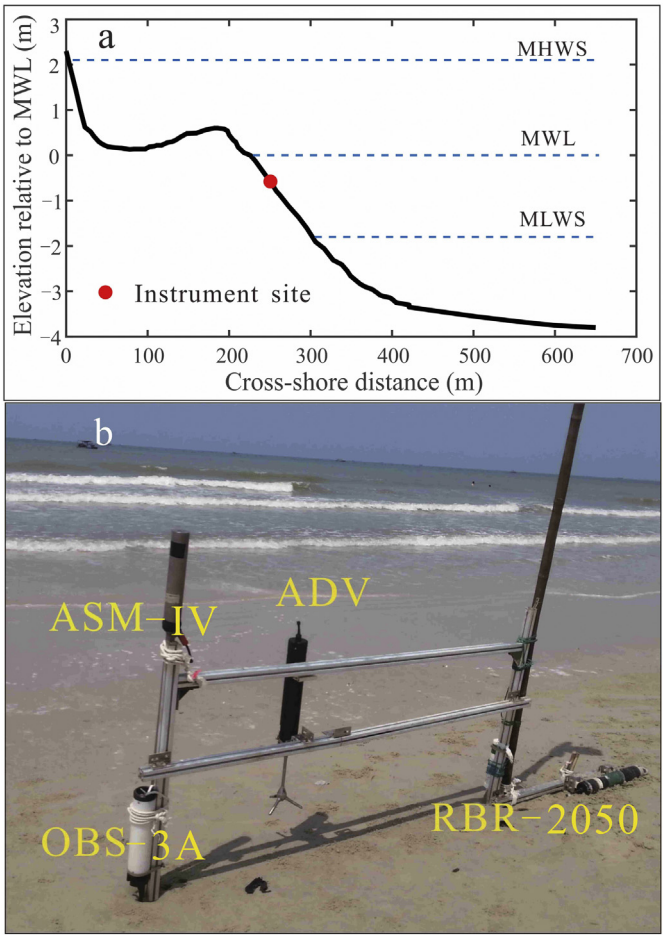

Fig. 2. (a) Beach profiles of Yintan Beach at the beginning of the measurement (x = 0 indicated location of sand dune) and locations of instrument sites, with red filled circles indicating instrument sites and blue dashed lines indicating mean high water in spring (MHWS), mean water level (MWL) and mean low water in spring (MLWS), respectively; (b) deployment of instrument rig. (For interpretation of the references to colour in this figure legend, the reader is referred to the web version of this article.)

Specifically, the ASM-IV was inserted vertically into the seabed and attached to an aluminum rod with several sensors buried in the sediment at the start of the observation to consistently obtain the SSCS in the area very close to the bed (Fig. 2b). The ASM-IV was logged at 1 Hz and obtained 96 vertical turbidity signals with a space interval of 1 cm. With this sample rate, the ASM-IV could continuously record turbidity data for 11.5 h due to a memory limitation. The ADV was fixed to the aluminum rod with the sensors facing downward and the measurement volume located approximately 4 cm above the bottom (called 'cmab' hereafter) at the beginning of the observation (Fig. 2b). The ADV was recorded at 64 Hz for 5 min every 10 min. The OBS-3A was fixed to the same rod as the ASM-IV and recorded the water depth for each minute, and its turbidity probe was at 4 cmab. Moreover, the RBR-2050 was attached to the other vertical pod close to the seabed and was logged at 4 Hz to record the pressure over a consecutive 512 s period every 20 min. Thus, there were 81 segments of 5 min synchronous measurement data (called 'burst' hereafter), including water depth, water surface elevation, high-resolution 3D flow velocity and near-bed vertical profile of SSCs, except when the instruments were exposed to the air at low tide and the ASM-IV missed the recorded data due to its memory limitation.

2.3. Methods

2.3.1. Extreme event statistics

Here, we identified the intermittent extreme events when the signals exceeded the 75th percentiles of the overall data for both TKE and SSC (i.e., TKE event and SSC event), although some researchers defined the extreme events by signals exceeding the mean plus one standard deviation (Cox and Kobayashi, 2000; Yoon and Cox, 2012) or only the mean values (Jaffe and Sallenger, 1992). Specifically, the threshold values of the 75th TKE and SSC events were 1.01 kg/ms^2 and 1.86 kg/m^3 at 4 cmab, respectively. The fractions of intermittent and correlated extreme events (defined as TKE events and SSC events occurred simultaneously) to the total time records and intermittent extreme event time records were defined as $^{n_1}/_{n}$ and $^{n_0}/_{n_1}$, respectively, where n is the

total number of data points for the TKE or SSC time series, n_1 is the number of data points exceeding the 75th percentile for the TKE or SSC time series, and n_0 is the number of data points where the TKE events and SSC events occurred synchronously. Thus, $^{n_0}/_{n}$ indicated the fraction of the time record that correlated extreme events occupied the total time records for TKE or SSC. Similarly, the percent of motions over the burst with respect to intermittent and correlated extreme events for TKE or SSC were defined as $^{n_1 m_1}/_{nm}$ and $^{n_0 m_0}/_{nm}$, respectively, where m is the mean value of the total data points, m_1 is the mean value of the data points of extreme events and m_0 is the mean value of data points referring to correlated extreme events.

2.3.2. Calculation of wave parameters

In this study, water surface elevation was reconstructed by linear wave theory from the pressure signal recorded by RBR-2050 (Gibbons et al., 2005), which provided a well estimation on wave parameters within 5% relative error compared with that using the weakly non-dispersive method of Bonneton et al. (2018) (full details of the comparison are provided in the Supporting Information, Text S2, Fig. S2, Table S1). Initial pressure signals recorded by RBR-2050 were removed the mean depths and detrended to obtain the hydrostatic-reconstructed η. Then the hydrostatic-reconstructed η was transformed to its frequency components by 1D real-only Discrete Fourier Transform. The pressure attenuation correction was conducted by multiplying the corresponding frequency components by the inverse of their attenuation due to depth of the RBR-2050 and overall depth of water. As a result, the reconstructed η was obtained by transforming the augmented frequency component into the time series with the Inverse Discrete Fourier Transform, during which the operation was limited to the detectable frequency band (i.e., between two cut-off frequency). To be specific, the minimum detectable frequency was calculated by sample rate divided by number of samples and maximum detectable frequency was determined by the lowest frequency whose pressure attenuation declined below 0.05. Afterwards, individual waves were identified by analyzing η with the zero-down crossing method and each single wave was divided into 20 points, accompanied by the time axis of each wave normalized with its period ($^{t}/_{T}$). Similarly, the time series of other hydrodynamic parameters (u, TKE and a) and SSC were also averaged over $^{t}/_{T}$, which is shown in the discussion section.

The dominant wave conditions were determined by the combination of relative wave height ($\frac{H}{h}$), wave shape skewness (Sk) and wave shape asymmetry (As), which were divided into the shoaling wave condition, breaking wave condition (generally corresponding to outer surf zone) and surf bore condition (generally corresponding to inner surf zone), respectively (Ruessink, 2010; Splinter et al., 2011; Grasso et al., 2012). Specifically, the $\frac{H}{h} < 0.3$ indicated a shoaling wave condition (non-breaking wave conditions) and $\frac{H}{h} > 0.3$ indicated a broken wave condition (generally corresponding to surf zone), while $\frac{H}{h} = 0.6$ ws the boundary that separates the wave conditions between breaking conditions and fully breaking conditions that are mainly subjected to surf bores. Moreover, a better method was proposed to separate breaking wave condition and surf bore condition by means of a $^{\mathrm{Sk}}/_{|\mathrm{As}|}$ ratio (Grasso et al., 2012) under conditions of $^{H_s}/_{h} > 0.3$. Specifically, $^{\mathrm{Sk}}/_{|\mathrm{As}|} > 1$ indicated breaking wave conditions, while $^{\mathrm{Sk}}/_{|\mathrm{As}|} < 1$ indicated surf bore conditions, of which the wave shape skewness was defined as follows:

$$\mathrm{Sk} = \frac{\overline{\eta_{inc}^3}}{\overline{\eta_{inc}^2}^{1.5}} \tag{1}$$

where the subscript *inc* represented η time series due to incident wave motion (0.05 < frequency < 0.5 Hz), and the bar above η indicated the average over an incident wave cycle.

The wave shape asymmetry was calculated by the following equation:

$$\mathrm{As} = \frac{\overline{\varkappa(\eta_{inc})^3}}{\overline{\eta_{inc}^2}^{1.5}} \tag{2}$$

where $\varkappa$ denoted the Hilbert transform (Elgar, 1987) of η.

2.3.3. TKE estimation

TKE was frequently used to detect the influence of turbulent flow motions on sediment suspension in the nearshore area (Foster et al., 1994; van der Werf et al., 2007; Yoon and Cox, 2012; Christensen et al., 2019). The TKE was estimated from the turbulent fluctuations by extracting the turbulent component from the high frequency horizontal and vertical velocities, and TKE was defined as follows (Stapleton and Huntley, 1995):

$$\mathrm{TKE} = \frac{1}{2}\rho(u'^2 + v'^2 + w'^2) \tag{3}$$

where u, v and w refer to the x, y and z components of velocity, respectively, and $'$ indicates the turbulent oscillation component. $\rho = 1025\ \mathrm{kg/m^3}$ was the seawater density. To obtain the turbulent component, the frequency cut-off method was used, depending on accurate determinations of the inertial velocity spectrum subrange (Foster et al., 2006). Among the methods proposed to determine the cut-off frequency, we chose the spectral slope breaks method (Smyth and Hay, 2003) to identify the inertial subrange of velocity data.

2.3.4. Calculation of both wave groupiness envelope and wave groupiness factor

The instantaneous wave groupiness envelope (ρ(t)) was estimated as follows (Veltcheva and Soares, 2016):

$$\rho(\mathrm{t}) = \sqrt{\eta^2(t) + \hat{\eta}^2(t)} \tag{4}$$

where η(t) indicated the water surface elevation from the mean water level, and $\hat{\eta}$(t) was the Hilbert transform of η, which was calculated by the following equation:

$$\hat{\eta}(\mathrm{t}) = \frac{1}{\pi}\mathrm{P}\int_{-\infty}^{\infty}\frac{\eta(t')}{t'-t}dt' \tag{5}$$

where P indicated the Cauchy principal value of the integral.

According to List (1991), the wave groupiness factor (GF_A) was defined as follows:

$$GF_A = \frac{\sqrt{2}\sigma_A}{\overline{A(t)}} \tag{6}$$

where A(t) was obtained by low-pass-filtering ρ(t) with a cut-off frequency of 0.05 Hz, while $\overline{A(t)}$ and σ_A were the mean and standard deviation of A(t) over two consecutive wave troughs, respectively.

2.3.5. Grey relational analysis method

Grey relational analysis (GRA) was an effective technique to solve the complicated interrelationship between multiple factors and variables within grey system theory (Deng, 1989; Balasubramanian and Ganapathy, 2011). GRA was used to compare the similarity between reference sequences and comparison sequences, so as to evaluate the relative importance of all factors to the system variables through grey relational degree (Deng, 1989; Huang and Huang, 1996). In recent years, it has been widely applied to biological processes, water quality evaluation, material science, computer science and so on (Tang et al., 1995; Chen and Syu, 2003; Chou and Tsai, 2009; Xu et al., 2011a, 2011b), because the factors used to evaluate complex systems are not necessarily independent of each other (Xu et al., 2011a, 2011b; Kadier et al., 2015). The limitation of GRA is that the resulting grey relational degree depends on the characteristics and numbers of other comparison sequences and therefore, all the possible influential factors should be contained in the GRA.

To evaluate the relative importance of various hydrodynamic forces,

including turbulence (TKE), waves (wave groups, incident wave and infragravity wave), horizontal pressure gradients (flow acceleration) and advection (mean current) on the time series of SSC, the GRA method was introduced to compare the similarities among SSC time series and TKE, wave groupiness envelope (A(t)), velocity due to incident wave (u_{inc}, bandpass filtering of u with cut-off frequency of 0.5 Hz and 0.05 Hz), velocity due to infragravity wave (u_{inf}, low-pass filtering of u with cut-off frequency of 0.05 Hz), flow acceleration (a) and mean current. The time series of SSCs was regarded as the reference sequence and was written as follows:

$$x_0 = \{x_0(k) \mid k = 1, 2, 3, ..., n\} \tag{7}$$

The comparison sequences were expressed as follows:

$$z_i = \{z_i(k) \mid i = 1, 2, ..., m; k = 1, 2, 3, ..., n\} \tag{8}$$

where n was the number of data points of each sequence, and m was the total number of comparison sequences. In this paper, $m = 6$ and $n = 300$ in consideration of the sample rate of ASM-IV over each 5-min interval.

However, for the convenience of the GRA, it was necessary to normalize the original comparison sequences. The calculated normalized sequences were expressed as follows:

$$x_i(k) = \frac{\max(z_i(k)) - z_i(k)}{\max(z_i(k)) - \min(z_i(k))} \tag{9}$$

Hence, the grey relational grade was analyzed by the following steps:

$$\Delta_{0i}(k) = |x_0(k) - x_i(k)| \tag{10}$$

$$\Delta_{min} = min_i min_k(\Delta_{0i}(k)) \tag{11}$$

$$\Delta_{max} = max_i max_k(\Delta_{0i}(k)) \tag{12}$$

$$\xi_{0i}(k) = \frac{\Delta_{min} + \rho\Delta_{max}}{\Delta_{0i}(k) + \rho\Delta_{max}} \tag{13}$$

$$\gamma_{0i} = \frac{1}{n}\sum_{k=1}^{n}\xi_{0i}(k) \tag{14}$$

where $\Delta_{0i}(k)$ was the matrix of the difference in absolute values between the reference sequence and normalized comparison sequences. Δ_{min} and Δ_{max} were the minimum and maximum values of matrix $\Delta_{0i}(k)$, ρ was a distinguishing coefficient that could be adjusted according to requirements, and this value was selected as 0.5 in this paper (Wong et al., 2006). $\xi_{0i}(k)$ represented the grey relational coefficients, while γ_{0i} was the grey relational grade, which was calculated by the averaged values of $\xi_{0i}(k)$. Thus, the influence degrees of TKE, wave groups, infragravity wave, incident wave, flow acceleration and mean current on the SSC time series can be obtained by the grey relational grade γ_{0i}.

3. Results

3.1. Characteristics of hydrodynamic conditions

During the observation when 81 synchronous bursts were recorded (i.e., except for the extreme low water period) from late 28th May to early 31st May, h ranged from 0.2 m to 2.2 m with decreasing tidal range (Fig. 3a). H_s ranged from 0.2 m to 0.6 m (Fig. 3b), and the significant wave period (T_s) varied between 3 s and 5.5 s over the observation time, with a relatively low T_s occurring at the start of the third tide (Fig. 3c). The maximum relative wave height ($^{Hm}/_{h}$, where H_m is the maximum wave height of each wave burst) varied from 0.2 near each high tide to 1.4 at low tide (h = 0.2 m) of the first tidal cycle (Fig. 3d). Moreover, both the mean cross-shore velocity (u) and alongshore velocity (v) ranged approximately ± 0.5 m/s, and the corresponding mean values during the observation were −0.05 m/s and −0.01 m/s, respectively (Fig. 3e and f).

Furthermore, as shown in Fig. 4a, the mean wave skewness (Sk) increased from 0 at $\frac{H}{h}$ = 0.05 to its maximum of 0.46 at $\frac{H}{h}$ = 0.55. Subsequently, the mean Sk tended to decrease with increasing $\frac{H}{h}$. On the other hand, when $\frac{H}{h}$ was lower than 0.3, As was positive and varied exponentially as $\frac{H}{h}$ increased (the information for As > 3 is not shown because it is beyond the scope of our discussion). As $\frac{H}{h}$ increased further, As showed negative values and continued to increase slowly in magnitude. Note that at the point of $\frac{H}{h}$ = 0.3, As changed from positive

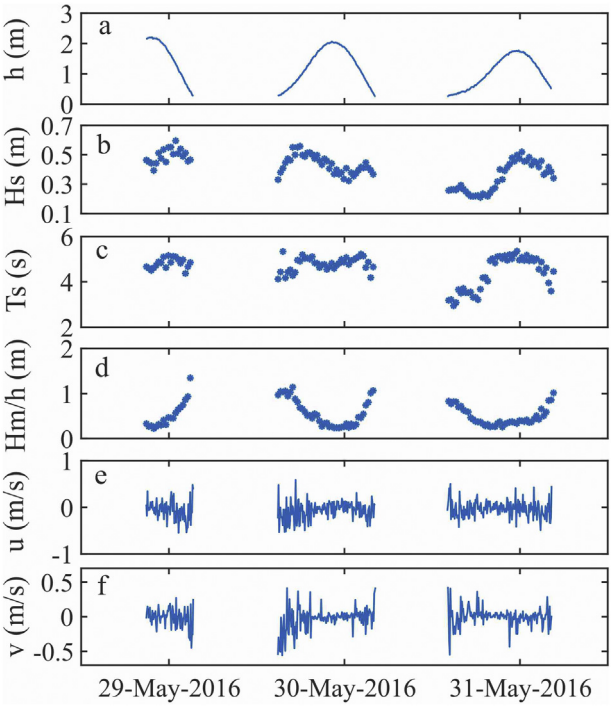

Fig. 3. Hydrodynamic conditions during the field measurement. (a) ~ (f) indicates water depth h, significant wave height H_s, significant wave period T_s, maximum relative wave height $^{Hm}/_{h}$, cross-shore velocity u and alongshore velocity v.

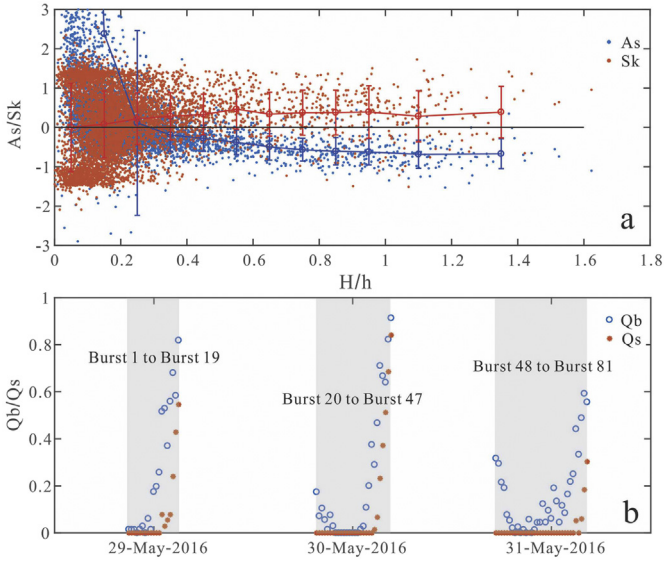

Fig. 4. (a) The variations in *As* and Sk versus the single relative wave height (H/h) for all the data points where the empty circle and vertical bar indicate the mean value ± standard deviation for the interval of 0.1H/h (except for the rightmost point); (b) fraction of breaking wave Q_b and surf bore Q_s of each burst. The grey areas in (b) indicate the distributions of 81 bursts.

to negative as $\frac{H}{h}$ increased, while $\frac{H}{h}$ = 0.6 was the transition point where|As|became larger than Sk (Fig. 4a). Hence, $\frac{H}{h}$ = 0.3 and 0.6 were the thresholds to separate the shoaling wave condition and broken wave condition, and the breaking wave condition and surf bore condition, respectively.

To better understand the hydrodynamic conditions of each burst, the fractions of broken waves (Qb, ratio of breaking wave and surf bore numbers ($\frac{H}{h}$ > 0.3) to total wave number of the burst) and surf bores (Qs, ratio of surf bore numbers ($\frac{H}{h}$ > 0.6) to total wave number of the burst) were calculated and are shown in Fig. 4b. Qb > 0 mainly occurred at low tide during the flood and ebb tides, and Qb reached 91% for Burst 47. Nonbreaking wave conditions occurred only at high tide with several bursts. In addition, the surf bore (Qs > 0) occurred for 18 of the 81 bursts at very low ebb tides, and the highest Qs of 85% occurred for Burst 47 (Fig. 4b).

Taken together, our measured data have encountered all three kinds of wave conditions (i.e., shoaling wave condition, breaking wave condition and surf bore condition). Considering that the three wave conditions may have different effects on the patterns of TKE and SSC distribution, three bursts from each kind of wave condition will be taken as examples for analyses hereafter.

3.2. Waves and wave groups under different wave conditions

To briefly compare the variations of incident waves and wave groups under different wave conditions, we selected three examples from the shoaling wave condition (Burst 27, Qb = 0), breaking wave condition (Burst 42,Qb = 0.47, Qs = 0.06) and surf bore condition (Burst 46, Qb = 0.82, Qs = 0.68) (Fig. 5) (Burst 47 was not used here because the lowermost probe of ASM-IV was intermittently emerged, though Qb = 0.91 in Burst 47).

Under the shoaling wave condition (Fig. 5a, d and g), η varied from −0.35 m to 0.35 m, and the water level fluctuation was obviously modulated by wave groups at time scales longer than 25 s, since the low-pass filtered wave groupiness envelope A(t) reflected the intensity of wave groups. The $\frac{H}{h}$ changed between 0.02 and 0.3 in relation to a single incident wave, and larger $\frac{H}{h}$ values occurred with the passage of larger wave groups (time = 50 s and 230 s with incident wave number = 12 and 55, respectively). Accordingly, the single wave period (T) fluctuated between 2.1 s and 6.6 s (Fig. 5d). Six complete wave groups occurred during Burst 27, and GF_A varied between 0.15 and 0.41, with a wave group period (T_{ig}) ranging between 27.8 s and 50.7 s (Fig. 5g).

Under the breaking wave condition (Fig. 5b, e and h), η ranged between −0.31 m and 0.40 m, and a significant difference occurred between the largest (time = 160 s) and smallest wave groups (time = 175 s). The $\frac{H}{h}$ values were no larger than 0.9, which was due to the further wave shoaling in shallow water, and larger $\frac{H}{h}$ values occurred similarly as the larger wave groups (Fig. 5e). T values were smaller than 6.6 s, and a very small T usually appeared following a small $\frac{H}{h}$ (Fig. 5e). GF_A values were > 0.1 and up to 0.5, while T_{ig} ranged between 24 s and 73 s (Fig. 5h). Moreover, there was large GF_A (0.51, wave group number = 3) under nonbreaking conditions (average relative wave height = 0.28, incident wave number ranged between 36 and 43), while quite small GF_A (0.11, wave group number = 4) occurred under breaking conditions (averaged relative wave height = 0.36, incident wave number ranged between 44 and 49).

Further into the surf bore condition (Fig. 5c, f and i), η ranged between −0.18 m and 0.27 m, and the incident waves became highly skewed and asymmetric. The maximum $\frac{H}{h}$ during the burst was 1.55, while the maximum T was > 10 s (Fig. 5f). Basically, T changed consistently with variations in $\frac{H}{h}$. Six wave groups occurred in the burst, with minimum and maximum T_{ig} values of 26 s and 60 s, respectively (Fig. 5i). As expected, the GF_A values ranged between 0.04 and 0.26, which were the smallest among the three wave conditions (Fig. 5i).

3.3. Variations in near-bed turbulent kinetic energy

Under the shoaling wave condition (Burst 27, Fig. 6a), TKEs were primarily smaller than 5 kg/ms^2, and high TKEs usually occurred under relatively high A(t) (time = 50 s and 230 s, Figs. 5a and 6a). The mean value of TKEs was 0.48 kg/ms^2, and most TKEs were lower than the threshold value of 1.01 kg/ms^2, which defined a TKE event (Fig. 6a). The low-pass-filtered TKEs indicated that relatively high TKEs occurred in the water column in the form of clusters, which corresponded well with the passage of large waves and wave groups (note the consistency between variations of low-pass-filtered TKEs (Fig. 6a) and A(t) (Fig. 5a)).

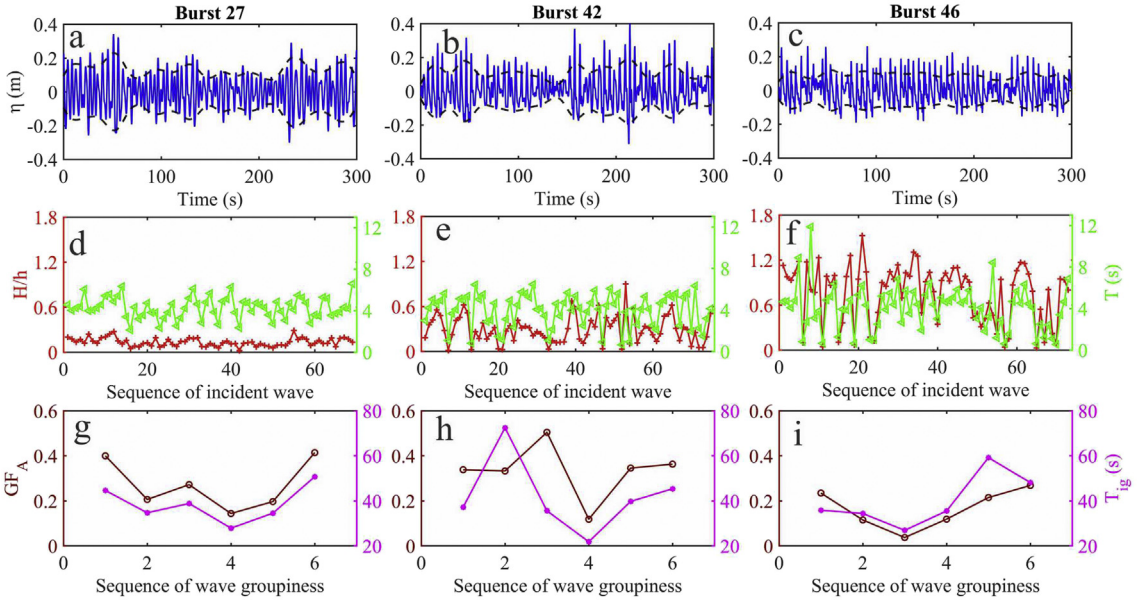

Fig. 5. Single wave and wave group variations for (a)(d)(g) Burst 27, (b)(e)(h) Burst 42, and (c)(f)(i) Burst 46 on behalf of shoaling wave condition, breaking wave condition and surf bore condition, respectively. Time series of (a)(b)(c) water surface elevation η and low-pass filtered wave groupiness envelope A(t) (black dashed line); Time series of (d)(e)(f) single relative wave height $\frac{H}{h}$ and single wave period T; Time series of (g)(h)(i) wave groupiness factor GF_A and wave group period T_{ig}.

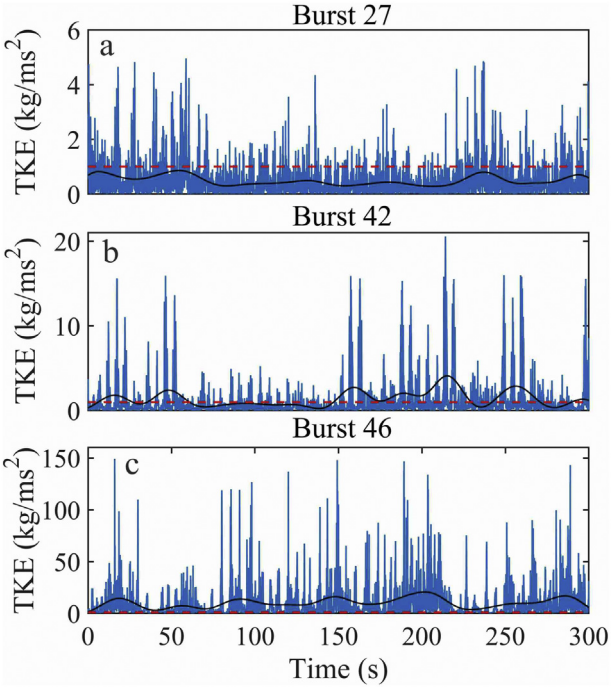

Fig. 6. Time series of turbulent kinetic energy TKE for (a) Burst 27, (b) Burst 42 and (c) Burst 46. Black lines indicate low-pass-filtered TKE with a cut-off frequency of 0.05 Hz. Red dashed lines indicate threshold values (1.01 kg/ms^2) of TKE events. (For interpretation of the references to colour in this figure legend, the reader is referred to the web version of this article.)

As the water depth decreased where the measurement point was located within the breaking point (Burst 42, Fig. 6b), TKEs became prominently larger than those in Burst 27, which was subject to shoaling wave conditions. The burst-averaged TKE in Burst 42 was 1.24 kg/ms^2, and the maximum TKE was up to 20.7 kg/ms^2 (Fig. 6b). Approximately 30% TKEs exceeded the threshold value of the TKE event (Fig. 6b). Similar to the variations in TKEs for Burst 27, the high TKE groups were produced within the passage of large wave groups (time = 50 s, 220 s and 260 s, Figs. 5b and 6b), which was confirmed by coincidence between low-pass-filtered wave groupiness envelopes and the corresponding low-pass-filtered TKEs (note the consistency between variations in low-pass-filtered TKEs (Fig. 6b) and A(t) (Fig. 5b)).

For Burst 46, where the water depth decreased further into the surf bore condition, TKE became extremely large compared to the situations for Burst 27 and Burst 42 (Fig. 6c, a and b). The maximum TKE was close to 150 kg/ms^2, and the mean value was equal to 10.1 kg/ms^2 (Fig. 6c), which meant that the water turbulent intensity within the surf bore condition was an order of magnitude larger than that under the breaking and shoaling wave conditions near the seabed of the measurement position. Moreover, the extreme TKE events occupied over 83% of the time records of TKEs (Fig. 6c).

3.4. Variations in suspended sediment concentrations

For Burst 27, as representative under the shoaling wave condition, the SSC time series at four vertical elevations within 10 cm (4 cmab, 6 cmab, 8 cmab and 10 cmab) showed similar variations, except at 2 cmab where persistent relatively high SSCs occurred approximately before time at 25 s (Fig. 7a). Specifically, at an elevation of 2 cmab, the SSC ranged from 1.0 kg/m^3 to 53.7 kg/m^3. When the elevation increased to 10 cmab, the corresponding SSCs decreased radically with respect to both the maximum (SSC = 6.5 kg/m^3) and minimum (SSC close to 0 kg/m^3) values, and the 5 min average SSC within 10 cm near-bed of the burst was 1.74 kg/m^3 (Fig. 7a). In addition, 10.7% of the SSC time records at 4 cmab were beyond the threshold of the SSC event of 1.86 kg/m^3. The other three SSC time series varied between the two time series described earlier (Fig. 7a). SSCs appeared in the form of clusters, and no phase lags occurred within 10 cm near-bed in terms of the peak SSC at different elevations, which was confirmed by the co-occurrence of maximum and minimum low-pass filtered SSCs at 2, 4 and 10 cmab (Fig. 7b, black and green vertical lines).

For Burst 42 (Fig. 7c), where data were recorded under the breaking wave condition, the SSCs apparently became larger for five elevations compared with those for Burst 27, which could be directly illustrated by the SSC time series at both 2 cmab (range of 1.6 to 54.8 kg/m^3) and 10 cmab (range of 0 to 15.6 kg/m^3), with a 5 min average SSC within 10 cm near-bed of 4.86 kg/m^3 (Fig. 7c). Moreover, the proportion of SSC time records at 4 cmab exceeding the threshold of the SSC event increased to 35%. In comparing the maximum and minimum values of low-pass-filtered SSCs at three elevations (Fig. 7d, black and green vertical dashed lines), the peak SSCs associated with wave groups within 10 cmab tended to be misaligned, which implied that multiple factors generated by breaking waves led to sediment resuspension and the consequential phase lags of SSCs at different elevations.

As the water depth decreased further into the surf bore condition (Burst 46, Fig. 7e), a significantly different pattern of SSCs was observed for Burst 46. Although the variation ranges of SSCs at 2 cmab were similar to those for Burst 40, the SSC time series at 10 cmab was obviously larger, with a peak SSC of 19.4 kg/m^3 for Burst 46. The 5 min-averaged SSC near the seabed (approximately 10 cm) under the surf bore condition was 7.72 kg/m^3, which was 1.5 and 4.5 times larger than those under breaking and shoaling wave conditions, respectively (Fig. 7a and c). Moreover, the proportion of SSC time records at 4 cmab exceeding the threshold of the SSC event increased to 74%, which suggested more vertical mixing of SSCs under the surf bore condition (Fig. 7e). Unlike the SSC variation patterns at different elevations under the shoaling and breaking wave conditions, misalignment of the maximum (and minimum) values of low-pass-filtered SSCs among the three elevations revealed the phase lags of vertical SSCs during Burst 46 (Fig. 7f, black and green vertical dashed lines).

4. Discussion

4.1. The influences of waves on TKEs

The TKE showed distinct variations under different wave conditions during the observation (Fig. 6). The mean TKEs near the bottom under the surf bore condition (Fig. 6c) were one order of magnitude larger than those under the shoaling condition (Fig. 6a) and were associated with the sources of turbulent eddies within different wave conditions according to the findings of Stansby and Feng (2005) and Nielsen et al. (2002). The mean TKEs under the breaking wave condition ranked between the two wave conditions (Fig. 6b) due to the partial surface-generated turbulence propagating downward the seabed (Svendsen, 1987). Considering that different wave conditions were separated by the level of relative wave height and that relative wave height was used to scale the nonlinearity of incident waves and the degree of breaking-wave intensity (Grasso and Ruessink, 2011; Aagaard et al., 2013; Christensen et al., 2019), $\frac{H}{h}$ may be a decisive indicator of the TKE intensity within the water column regardless of wave conditions. As expected, this assumption was confirmed by good correlation coefficients between TKE and single $\frac{H}{h}$ for different wave conditions (R = 0.41, 0.53 and 0.46 for Fig. 8a, b and c, respectively) and all bursts (81) (Fig. 8d). In fact, the larger the wave heights were, the stronger the water turbulence in the near-bed induced by friction between wave orbital motion and the seabed (Nielsen et al., 2002). Moreover, the shallower the water depths were, the weaker the wave attenuation along the path downward the seabed (Gibbons et al., 2005); this situation was accompanied by wave transformation from shoaling

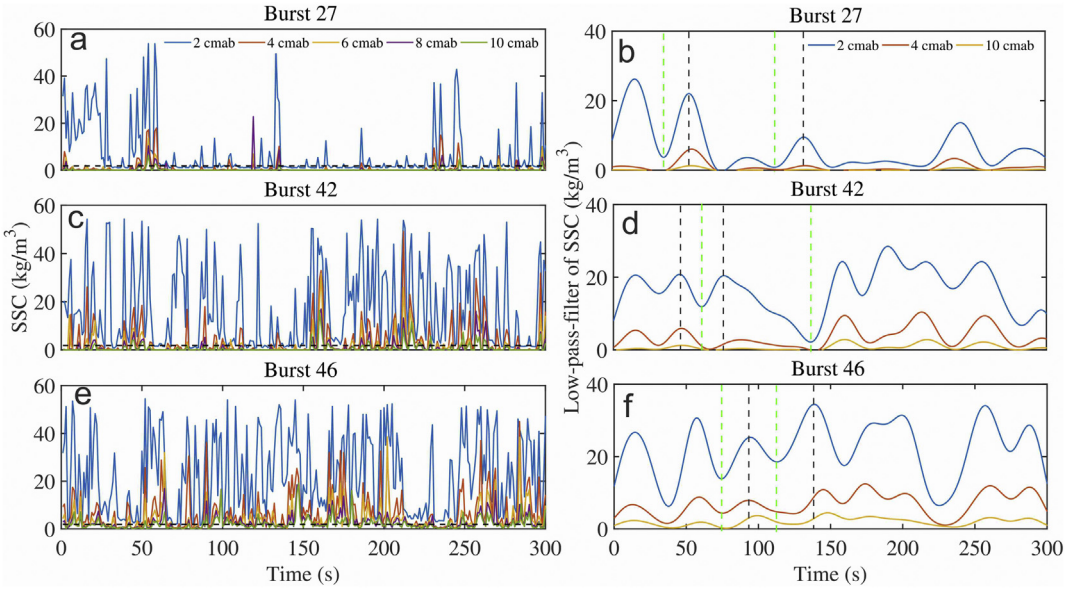

Fig. 7. Time series of SSC for (a) Burst 27, (c) Burst 42 and (e) Burst 46 at elevations of 2 cmab, 4 cmab, 6 cmab, 8 cmab and 10 cmab, respectively. Low-pass-filtered SSC with a cut-off frequency of 0.05 Hz for (b) Burst 27, (d) Burst 42 and (f) Burst 46 at elevations of 2 cmab, 4 cmab and 10 cmab, respectively. Black dashed lines at (a) (c) and (e) indicate threshold values (1.86 kg/m^3) of SSC events. Black and green vertical dashed lines at (b) (d) (f) indicate the occurrences of maximum and minimum low-pass-filtered SSCs at 2 cmab, respectively. (For interpretation of the references to colour in this figure legend, the reader is referred to the web version of this article.)

to breaking waves and surf bores when the water depth was lower than the breaker depth, and both conditions would improve the turbulence intensity by means of bed and surface-generated turbulent eddies (Stansby and Feng, 2005). Hence, combining the impacts of wave height and water depth explained that more near-bed turbulent eddies were produced from both the seabed and the water surface as the relative wave height increased shoreward.

Wave groups could play an important role in TKE due to the structure coupling between smaller waves and antecedent larger waves under the passage of wave groups (Villard et al., 2000). However, in this study, there was no statistically significant relationship between TKE and the intensity of wave groups (GF_A) with poor correlations for both shoaling wave conditions (R = 0.27) and broken wave conditions (R = -0.21) (Fig. 8e and f). Meanwhile, a negative correlation between GF_A and the corresponding TKE was found under the broken wave condition, which might be ascribed to wave breaking and the resulting surface-generated turbulence (Stansby and Feng, 2005; Dong et al., 2008). Based on the lagged correlation analysis between A(t) and low-pass-filtered TKEs (Fig. 8g), the variations in TKE were mainly one wave period (wave period ranged from 3 s to 5.5 s) lagged behind wave

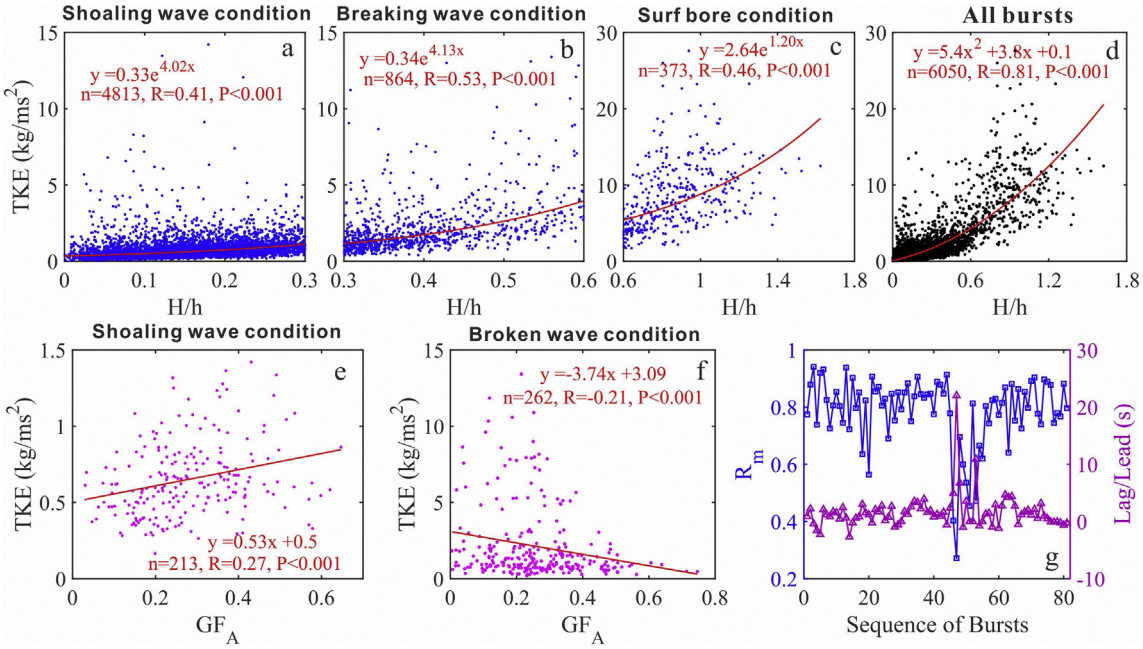

Fig. 8. Mean TKE against H/h under (a) shoaling wave condition, (b) breaking wave condition, (c) surf bore condition, and (d) for all bursts (81) covering the three wave conditions. Mean TKE against GF_A under (e) shoaling wave condition and (f) broken wave condition. (g) Best correlation coefficient R_m and lag/lead time of lagged correlations analysis between A(t) and low-pass-filtered TKE of each burst.

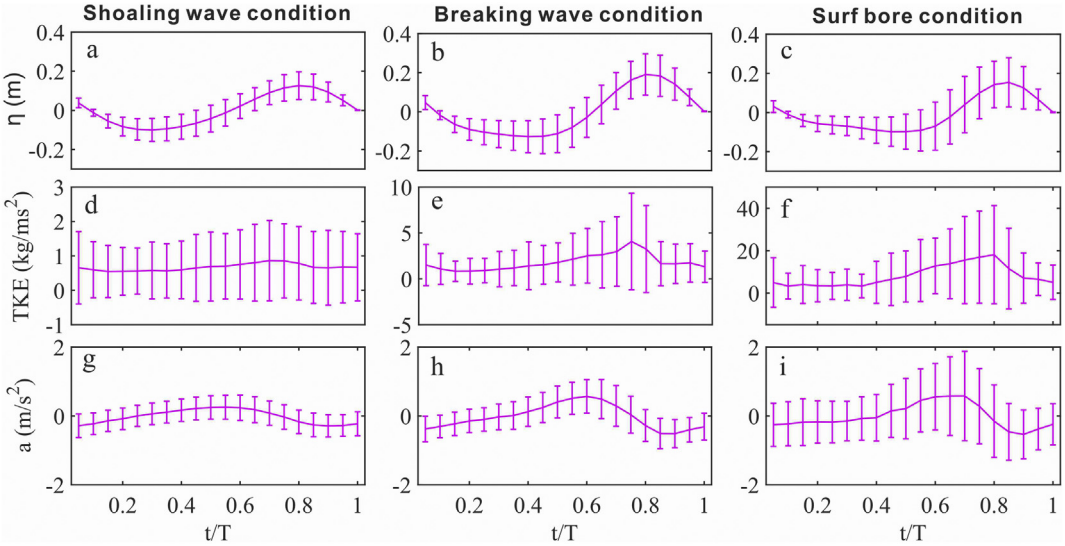

Fig. 9. Phase-averaged (a)(b)(c) η of a single wave, (d)(e)(f) TKE and (g)(h)(i) flow acceleration an under shoaling wave condition, breaking wave condition and surf bore condition, respectively. Vertical bars indicate the mean ± standard deviation.

groups with delay times varying from −2.3 s to 4.7 s. The reason of the lagged relations between low-pass-filtered TKEs and wave groups were the continual ejection of turbulence associated with wave pumping and vortex releasing processes (Vincent and Hanes, 2002). Notably, both the lag time and best correlation coefficients of Burst 47 and Burst 53 (Fig. 8g) were abnormal which may be associated with massive wave breaking-induced bubbles (Qb = 0.91 for Burst 47, Fig. 4b) and changing wind wave climate (relatively low T_s for Burst 53, Fig. 3c, Fig. 4b) that might break the coupling relationship between wave groups and TKE (Grasso and Ruessink, 2011).

Furthermore, by phase-averaged analysis, temporal differences in TKEs within the intrawave scale were directly illustrated by the phase-averaged process (Fig. 9). Specifically, larger TKEs occurred at approximately 0.55–0.75 t/T (at the wave front), and mean TKEs peaked at the wave front, 0.05 to 0.1 t/T ahead of the wave crest, especially for the cases of the breaking wave condition and the surf bore condition, while the TKE was not obviously larger in the wave front under the shoaling wave condition (Fig. 9d, e and f). In these cases, for the shoaling wave condition, the relatively high TKE at the wave front may have been due to ejection of the turbulent vortex from the bed at the flow reversal in the wave front, which was related to the evolution of the wave boundary layer (Fig. 9d) (van der Werf et al., 2007; Christensen et al., 2019). Under the breaking wave condition, the distribution of high mean TKE > 1.01 kg/ms^2 (Fig. 9e) was associated with a rapid increase in the cross-shore pressure gradient-induced disturbance of the wave boundary layer at the wave front due to near-breaking waves (Nielsen, 2006; Nichols and Foster, 2007). Further into the surf bore condition, a higher mean TKE > 1.01 kg/ms^2 occurring within the wave front was primarily ascribed to the influence of surface-generated turbulent eddies (Butt et al., 2004; Christensen et al., 2019).

Noting that all three mechanisms of explanation were related to flow acceleration (Drake and Calantoni, 2001; Butt et al., 2004), attention should be paid to the characteristics of the intrawave a variation. As shown in Fig. 9g, h and i, larger mean a values occurred in the wave front (t/T = 0.55 to 0.75) for the breaking wave condition (0.58 m/s^2) and surf bore condition (0.59 m/s^2), while the mean a that occurred in the wave front (0.26 m/s^2) was approximately equal to that in the wave rear (−0.28 m/s^2) for the shoaling wave condition. A larger peak a still existed in the surf bore condition, as the average a plus one standard deviation for the surf bore condition reached 1.9 m/s^2 (Fig. 9i, $^t/_T$ = 0.7), while that for the breaking wave condition was smaller than 1.1 m/s^2 (Fig. 9h, $^t/_T$ = 0.6), although the mean values were approximately identical at 0.6 m/s^2. The consistency of occurrence between the large phase-averaged TKE and peak a implied that flow acceleration played an important role in the generation of turbulence at the moment of flow reversal for different wave conditions (van der Werf et al., 2007; Nichols and Foster, 2007; Murray et al., 2011) Moreover, the assumption that the flow acceleration contributed to the ejection of the turbulent vortex was directly suggested by the good correlation coefficient (R = 0.53, Fig. 10) between the peak a of a single wave and the synchronous TKE in Fig. 10. The possible reason was that when the flow acceleration was large, the boundary layers had little time to develop and a high intensity of turbulence was generated (Nielsen, 2006). Hence, flow acceleration might act as a proxy for turbulence in terms of the sediment transport mechanism (Puleo et al., 2003; Austin et al., 2009).

4.2. The influences of waves on SSCs

Incident waves have been confirmed to act as a stirring mechanism of sediment suspension, making the event of sediment suspension occur at the time scale of a half wave or incident wave (Dally and Dean, 1984; Williams et al., 2002). In this study, the mean SSC, in terms of a single wave, was well correlated (R = 0.45) with $\frac{H}{h}$ under the shoaling wave condition (Fig. 11a), which indicated that the SSC could be estimated by $\frac{H}{h}$. However, further into the surf zone where waves were broken, correlations between them became relatively poor (R = 0.25 and 0.12,

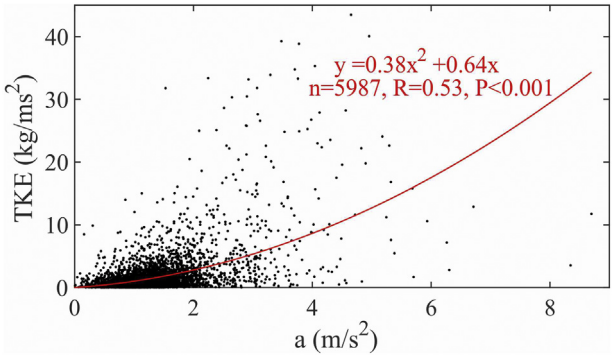

Fig. 10. Synchronous TKE against peak flow acceleration a of a single wave for all the data points.

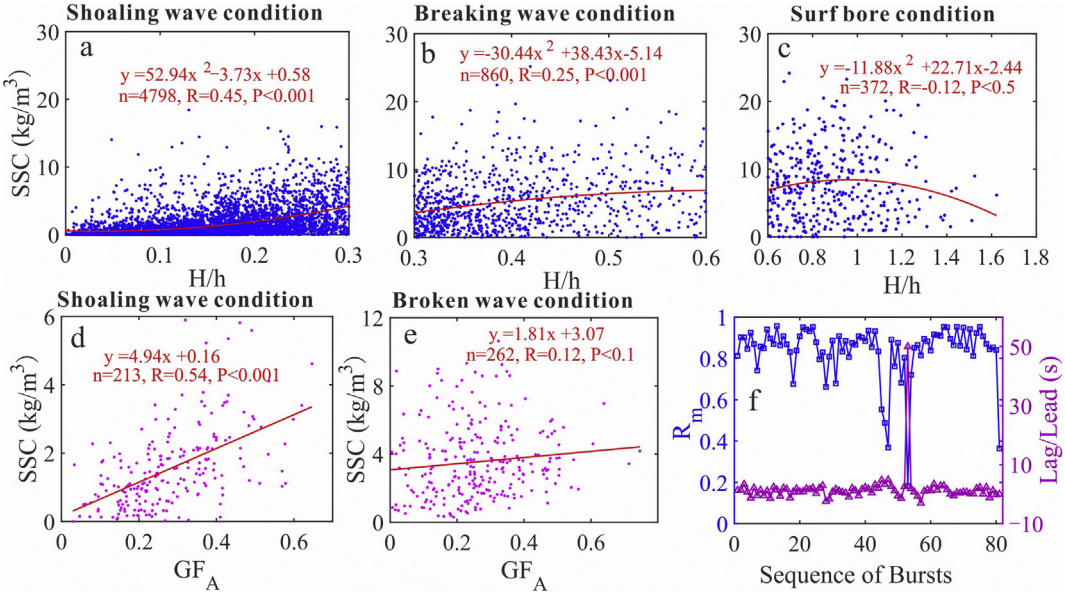

Fig. 11. Mean SSC against H/h under the (a) shoaling wave condition, (b) breaking wave condition and (c) surf bore condition. Mean SSC against GF_A under (d) shoaling wave condition and (e) broken wave condition. Best correlation coefficient R_m and lag/lead time of lagged correlations analysis between A(t) and low-pass-filtered SSC of each burst.

respectively), especially under surf bore condition (Fig. 11b and c). Therefore, the factors controlling sediment suspension became more complicated under broken wave condition (within the surf zone), where factors including undertow, infragravity wave, surf bores and even infiltration/exfiltration processes could make significant differences (Aagaard and Greenwood, 1995; Longo et al., 2002; Butt et al., 2004).

An analysis of intrawave SSC variation needs to be conducted to determine the characteristics of sediment suspension under different wave conditions for further exploration of the corresponding mechanism. As shown in Fig. 12g, h and i, the phase-averaged SSCs under the surf bore condition were obviously larger than those under the breaking and shoaling wave conditions, with peak mean values of 13.6 kg/m^3, 11.5 kg/m^3 and 3.75 kg/m^3, respectively. Combined with the statistics of mean SSC under different wave phases (Table 1), it was preliminarily inferred that phase-averaged peak SSCs were coincident with the lowest surface water elevation and the largest negative u over a normalized wave cycle regardless of wave conditions (Fig. 12). Some previous measurements found that two peak SSCs dominated each wave half-cycle in laboratory and field experiments (Nakato et al., 1977; Villard and Osborne, 2002; Murray et al., 2011; Ruessink et al., 2011).

Table 1
Averaged SSCs at an elevation of 4 cmab at different wave phases under the shoaling wave condition (relative wave height < 0.3), breaking wave condition (0.3 < relative wave height < 0.6) and surf bore condition (relative wave height > 0.6).

	SSC (kg/m^3)			
	Wave trough	Zero-up	Wave crest	Zero-down
Shoaling wave condition	2.8 ± 4.5	1.4 ± 2.2	0.6 ± 1.4	0.8 ± 1.8
Breaking wave condition	9.7 ± 8.1	4.2 ± 4.3	1.3 ± 1.9	2.3 ± 2.9
Surf bore condition	11.6 ± 8.8	6.9 ± 5.9	3.4 ± 4.2	4.3 ± 4.8

Note: Data are shown as the mean value ± standard deviation.

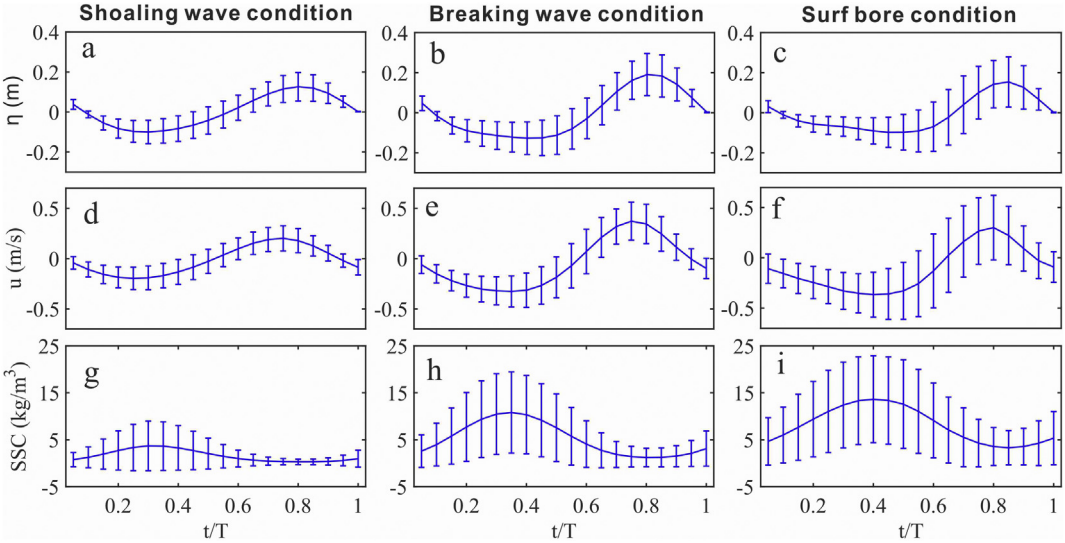

Fig. 12. Phase-averaged (a)(b)(c) η of single wave, (d)(e)(f) cross-shore velocity u and (g)(h)(i) SSC under shoaling wave condition, breaking wave condition and surf bore condition, respectively. Vertical bars indicate the mean ± standard deviation.

Among these studies, the occurrence of two peaks at times of flow reversal was attributed to energetic turbulent eddies due to flow separation. In addition, some measurements only captured one peak SSC during incident wave cycles, during which the peak SSC could occur either in the onshore phase (O'Donoghue and Wright, 2004; Brinkkemper et al., 2017) or in the offshore phase of the wave cycle (Osborne and Greenwood, 1993; Kularatne and Pattiaratchi, 2008). The researchers attributed this phenomenon to higher velocity-induced bed shear stress in the onshore phase of the wave cycle or to the influence of vortex ripples, respectively (O'Donoghue and Wright, 2004; Aagaard and Jensen, 2013). However, in this study where the peak SSCs always occurred in association with the wave trough, the occurrence of the peak SSC relative to the wave phase may be due to the influence of ripple morphology under the condition that the peak flow velocities at wave crest and wave trough were close to each other, as suggested by Aagaard and Jensen (2013). When incident waves propagated over sand ripples, sediments were entrained near the seabed due to onshore-directed velocity and sand-laden vortices were formed on the lee sides of the ripples during the onshore phase of wave motions. Then the sand-laden vortices were released and ejected to higher elevations as the flow reversed (Inman and Bowen, 1963; Vincent et al., 1991). Eventually, high SSCs were transported seaward under offshore-directed flow, which was coupled with the offshore wave phase. To further examine the relationship between the wave and peak SSC within the intrawave scale, curve fittings with regard to peak SSC and the u and η values over each incident wave cycle were conducted and were shown in Fig. 13. A good correlation between peak SSC and simultaneous u (R ranging from -0.51 to -0.60, $P < 0.001$) and η (R ranging from -0.50 to -0.55, $P < 0.001$) for all three wave conditions indicated that near-bed peak SSCs were associated with the phase of the incident wave in which the wave trough occurred.

Wave groups were previously shown to enhance sediment suspension and increase the following SSCs at higher free stream elevations (Hanes and Huntley, 1986; Lee et al., 1994; Murray et al., 2012). There was a good correlation coefficient ($R = 0.54$, Fig. 11d) between GF_A and SSC under the shoaling wave condition in this study, which indicated a significant contribution to SSCs from the wave groups. However, wave groups may act as a less important factor in controlling the SSC under broken wave condition (within surf zone) relative to the surf bore and undertow, which was clearly illustrated by the poor correlation coefficient ($R = 0.12$, Fig. 11e) between GF_A and SSC. Furtherly, both the surface-generated large-scale turbulence (surf bores) and the offshore-directed undertow, a balance to compensate the wave-induced onshore mass transport, greatly contributed to sediment suspension (Roelvink and Stive, 1989; Aagaard and Hughes, 2010) along with wave energy dissipation and wave deformation through surf zone (Raubenheimer et al., 1996). Moreover, low-pass-filtered SSCs primarily lagged behind the wave groupiness envelope, with a lag time between -3 s and 4.9 s, during which only 17 bursts showed a negative lagged times (Fig. 11f). Notably, poor correlation coefficients occurred for Burst 45, Burst 46, Burst 47 and Burst 81 resulting from surf conditions, which coincided with Fig. 11d. In addition, the lag time of Burst 53 was abnormal since the relationship between the wave groups and TKE may have been broken due to the change in the wind wave climate depicted previously (Grasso and Ruessink, 2011).

4.3. Coupling between TKEs and SSCs

Intermittent and correlated extreme events of TKE and SSC statistics over 81 bursts were conducted and are shown in Fig. 14. The fraction of SSC events ($^{n_1}/_{n}$) ranged from 10% for Burst 54 to 75% for Burst 47 (Fig. 14a). However, the percentage of SSC records ($^{n_1 m_1}/_{nm}$) remained at high levels (from 69% for Burst 4 to 99% for Burst 81) over all bursts. The fraction of correlated extreme events to SSC events ($^{n_0}/_{n_1}$) varied from 3% for Burst 23 to 95% for Burst 47. In addition, the percentage of correlated extreme events to SSC records ($^{n_0 m_0}/_{nm}$) ranged between 2% for Burst 23 and 95% for Burst 46. Additionally, $^{n_1}/_{n}$, $^{n_0}/_{n_1}$ and $^{n_0 m_0}/_{nm}$ of TKE showed similar variation patterns to SSC, as well as qualitative variation in proportion to Qb (Figs. 4b, 14), and the corresponding variation ranges were 3% for Burst 26 to 100% for Burst 47, 10% for Burst 23 to 74% for Burst 47, 2% for Burst 28 and Burst 61 to 76% for Burst 46, respectively (Fig. 14b). Unlike the variation pattern of $^{n_1 m_1}/_{nm}$ in the SSC, the corresponding values of TKE varied in accordance with Qb with a variation between 16% for Burst 26 and 100% for Burst 47.

The average TKE events and SSC events occupied 31.1% and 28.5% of the corresponding time record and contained up to 78.2% and 90.1% of motions, respectively (Table 2). The standard deviation of $^{n_1 m_1}/_{nm}$ for the SSC (7.1%) was much smaller than that of TKE, which indicated

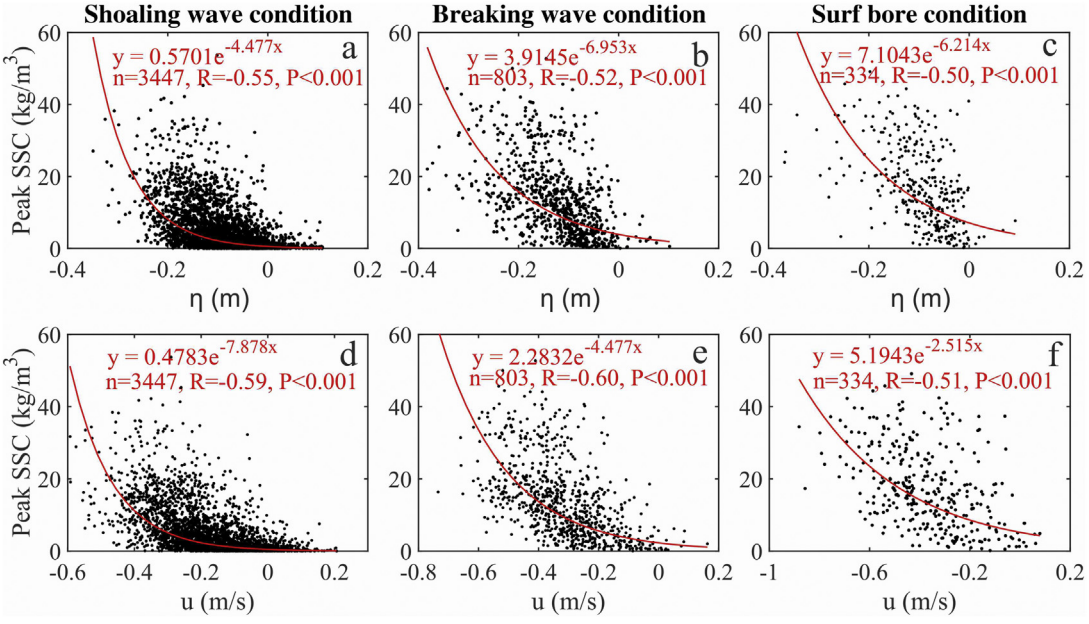

Fig. 13. (a) and (d) indicate the best fit between the peak SSC and water surface elevation η and cross-shore velocity u under shoaling wave condition, respectively; (b) and (e) indicate the best fit between the peak SSC and water surface elevation η and cross-shore velocity u under breaking wave condition, respectively; (c) and (f) indicate the best fit between peak SSC and water surface elevation η and cross-shore velocity u under surf bore condition, respectively.

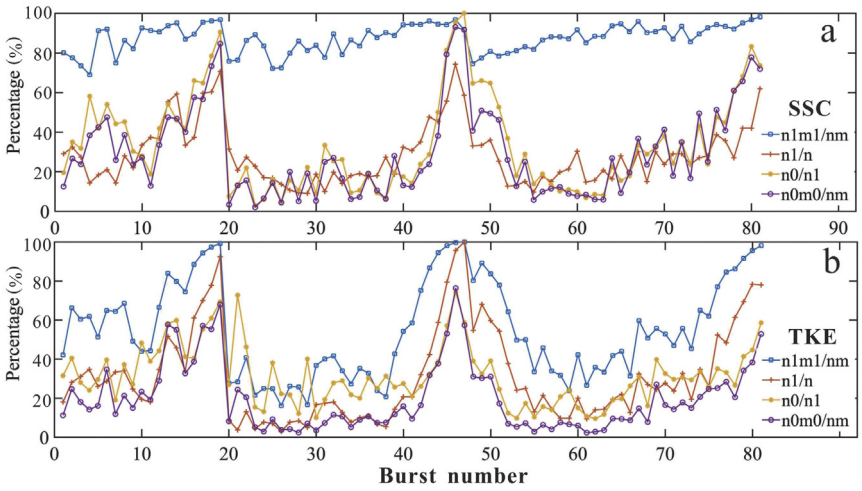

Fig. 14. (a) The fractions of SSC events to the total time records ($^{n1}/_{n}$) and correlated extreme events to the intermittent SSC events ($^{n0}/_{n1}$), and the percent of SSC events to the total sediment concentrations ($^{n1m1}/_{nm}$) and correlated extreme events to the total sediment concentrations ($^{n0m0}/_{nm}$). (b) The fractions of TKE events to total time records ($^{n1}/_{n}$) and correlated extreme events to intermittent TKE events ($^{n0}/_{n1}$), and the percent of TKE events to the total turbulent motions ($^{n1m1}/_{nm}$) and correlated extreme events to the total turbulent motions ($^{n0m0}/_{nm}$).

that not all the TKEs in the water column contributed to sediment suspension (Alsina and Cáceres, 2011; Yoon and Cox, 2012). The correlated extreme events accounted for 39.0% and 42.9% of records with respect to TKE events and SSC events on average, respectively, and low fractions of correlated extreme events were illustrated by the intrawave variations in SSC and TKE (Figs. 9g, h, i, 12g, h and i). However, the correlated extreme events contained 38.1% and 40.0% of the total turbulence motions and suspended sediment concentrations, respectively, under the conditions that correlated extreme events occurred during only 12.2% of the time series for both TKE and SSC. Hence, this finding implied that approximately 40% of sediment suspension motions were associated with turbulent motions and that approximately 38% of turbulent motions contributed to sediment suspension, even though only 12% of data time records ($^{n0}/_{n}$) were occupied for the SSC and TKE time series, which was consistent with the findings of Cox and Kobayashi (2000) and slightly lower than the findings of Yoon and Cox (2012). The results indicated that parts of TKEs dissipated directly in the water column rather than suspended the sediments while sediment motions were partly induced by other physical processes, not restricted to turbulent motions.

Based on the contribution of TKE to SSC, the relationship between TKE and SSC was further examined in terms of the incident wave time scale and wave group time scale. As shown in Fig. 15a, b and c, the correlation between the single wave-mean TKE and SSC was poor under the shoaling wave condition (R = 0.28), while TKE and SSC were considered to be unrelated under the breaking wave (R = -0.08) and surf bore (R = 0.09) conditions. The statistics that show the contribution of TKE to SSC increased proportionally with Qb, which was contrary to the relationship between TKE and SSC among different wave conditions, and this result may have occurred because the threshold values of extreme events were calculated based on all bursts (81). However, with respect to the time scale of the wave group, the mean SSCs were highly correlated with the mean TKE whether under the shoaling wave condition (R = 0.58, Fig. 15d) or the broken wave condition (R = 0.69, Fig. 15e). Thus, we deduced that it was more effective for TKE to contribute to sediment suspension at the time scale of the wave group than at the incident wave scale.

4.4. Relative significance of waves and TKE to suspended sediment concentration

To evaluate the relative significance of different forces for the variations in the SSC time series, the GRA method was carried out. The grey relational grades of TKE (γ_{01}), wave groupiness envelope (γ_{02}), velocity due to infragravity wave (γ_{03}), velocity due to incident wave (γ_{04}), flow acceleration (γ_{05}) and mean current (γ_{06}) that reflect the relative effects of the turbulence, wave groups, incident wave, infragravity wave, horizontal pressure gradients and advection on SSC, respectively, are compared in Fig. 16. From the results, we determined that γ_{01}, which ranged from 0.73 to 0.93, was always larger than the other five grey relational grades for all bursts (81). For all bursts, we noted that both γ_{02} (ranging from 0.47 to 0.75) and γ_{05} (ranging from 0.52 to 0.68) exceeded γ_{03} (0.48 to 0.62), γ_{04} (0.51 to 0.63) and γ_{06} (0.50 to 0.62) for most bursts (Fig. 16). In addition, the mean γ_{01} of 0.82 was highest among the six grey relational grades (Table 3). Both the mean γ_{02} and γ_{05} were equal to 0.58 and slightly exceeded 0.55, which was the mean value of γ_{03}, γ_{04} and γ_{06} (Table 3). From the perspective of wave conditions, the relative importance of different hydrodynamic forces had changed obviously. Under shoaling wave conditions, it was still suggested that TKE (γ_{01}) played the most important role in the variations of SSC time series (i.e., sediment suspension) among the hydrodynamic factors, followed by the wave group (γ_{02}) and flow acceleration (γ_{05}), while the single wave (including the incident wave (γ_{03}) and infragravity wave (γ_{04})) and advection (mean current, γ_{06}) slightly ranked last (Table 3). However, under broken wave conditions (bursts dominated by breaking waves and surf bores),

Table 2
Statistical average of extreme events of overall bursts (81).

Coherent events	$\overline{n1/n}$ (%)	$\overline{n1m1/nm}$ (%)	$\overline{n0/n1}$ (%)	$\overline{n0/n}$ (%)	$\overline{n0m0/nm}$ (%)
TKE	31.3 ± 24.1	78.2 ± 24.7	39.0 ± 15.3	12.2 ± 15.1	38.1 ± 17.2
SSC	28.5 ± 14.9	90.1 ± 7.1	42.9 ± 23.9	12.2 ± 15.1	40.0 ± 22.6

Note: Data are shown as the mean value ± standard deviation.

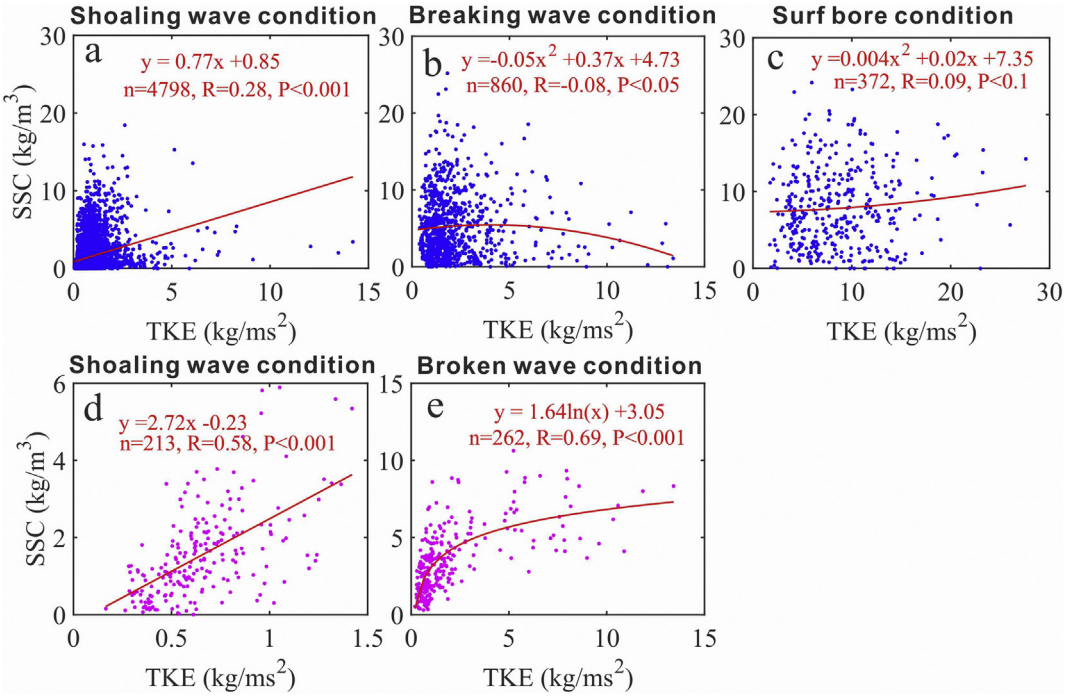

Fig. 15. Mean SSC against mean TKE in terms of incident wave time scale under (a) shoaling wave condition, (b) breaking wave condition and (c) surf bore condition. Mean SSC against TKE at the wave group time scale under (d) shoaling wave condition and (e) broken wave condition.

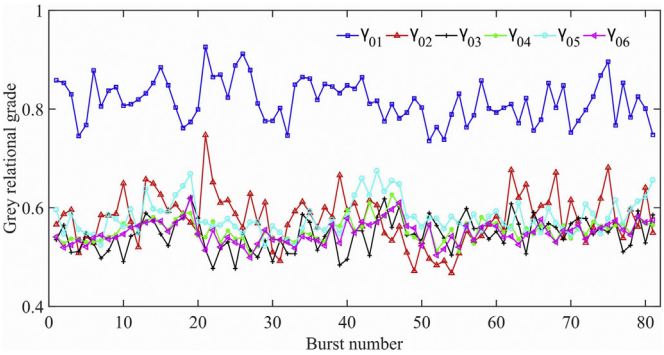

Fig. 16. Grey relational grades of TKE (γ_{01}), low-pass-filtered wave groupiness envelope A(t) (γ_{02}), velocity due to infragravity wave (γ_{03}), velocity due to incident wave (γ_{04}), flow acceleration (γ_{05}) and mean current (γ_{06}) to SSC for each burst.

the relative importance of flow acceleration for variations in SSCs improved significantly (mean γ_{05} = 0.65) while the four hydrodynamic forces (grey relational grades varied between 0.58 and 0.59, expect for TKE) were considered equivalent factors to the contributions to SSCs. Thus, we deduced that TKE played the most important role in the variations in SSC time series (i.e., sediment suspension) among the hydrodynamic factors irrespective of wave conditions and that flow acceleration played the second most important role under broken wave conditions while the wave group, single wave (including the incident wave and infragravity wave) and advection (mean current) were considered equivalent and less important factors in terms of our measured data.

The deduction that turbulence played the most important role in sediment suspension among most hydrodynamic factors (γ_{01} was largest) was consistent with the results of Osborne and Greenwood (1993) who observed that higher suspension events were caused by turbulence. Our results therefore supported that SSC could not be well predicted by the wave velocity (Jaffe and Rubin, 1996), as well as the observation that the seabed configuration served as a secondary factor relative to oscillatory wave motions in terms of sediment suspension (e.g., Sternberg et al., 1985; Osborne and Greenwood, 1992). Meanwhile, the greater contribution to sediment suspension from wave group (γ_{02}) than single wave (γ_{04} and γ_{03}) under the shoaling wave condition (Table 3) could be verified by the finding of Williams et al. (2002) who showed that sediment suspension was more prominent at the time scale of wave group than at the incident wave frequency band. Moreover, γ_{05} and γ_{06} were relatively large for Burst 19 (0.67 and 0.62) and Burst 47 (0.65 and 0.61) (Fig. 16) where Qb was accordingly high (0.82 and 0.91, respectively, Fig. 4b). It could thus be concluded that there were greater contributions to sediment suspension from flow acceleration and advection (mean current) due to highly skewed and asymmetric breaking waves and strong breaking wave-induced mean current in the high-

Table 3
Statistical grey relational grades of TKE (γ_{01}), low-pass-filtered wave groupiness envelope (γ_{02}), velocity due to infra-gravity (γ_{03}), velocity due to incident wave (γ_{04}), flow acceleration (γ_{05}) and mean current (γ_{06}) relative to SSC under different wave conditions and for all bursts (81).

	Comparison sequences					
	γ_{01}	γ_{02}	γ_{03}	γ_{04}	γ_{05}	γ_{06}
All bursts	0.82 ± 0.04	0.58 ± 0.05	0.55 ± 0.03	0.55 ± 0.02	0.58 ± 0.03	0.55 ± 0.02
Shoaling wave condition	0.82 ± 0.04	0.59 ± 0.06	0.53 ± 0.03	0.54 ± 0.02	0.58 ± 0.02	0.54 ± 0.02
Broken wave condition	0.79 ± 0.04	0.58 ± 0.04	0.58 ± 0.03	0.59 ± 0.02	0.65 ± 0.03	0.58 ± 0.02

Note: Data are shown as the mean value ± standard deviation.

energy dissipative surf zone, which provides new evidence to support the previous view proposed by Aagaard and Greenwood (2008). Moreover, the effects of the environment including sediment grain size, beach slope and seabed configuration (erosion/deposition, bed ripple) would also influence sediment suspension and the resulting SSCs (Longuet-Higgins and Stewart, 1964; Osborne and Greenwood, 1993; Masselink et al., 2007a, 2007b; Bertin et al., 2018), which were not reflected in the process of GRA. In fact, the sediment grain size on the surface of the measurement site varied from 0.14 mm to 0.20 mm (fine sand) across the intertidal region, and such a small variation in grain size would not significantly change the relationship among TKE, waves and SSC. Moreover, the beach slope was approximately 2.5%, and it might have remained unchanged during the observations according to a previous study (Pang et al., 2019) that was conducted in the same position and under similar wave conditions. Hence, the stable beach slope would also not affect the mechanism of sediment suspension. In addition, the measured position generally exprienced a slight erosion/deposition rate (Capo et al., 2009; Ge et al., 2017). Therefore, the inconspicuous changes in beach elevation would not disorder the relative importance of different hydrodynamic forces. Note that the variation in the beach slope is consistent with the sediment grain size (generally, the sediment grain size is large where the beach slope is steep and vice versa). Thus, for other coastal environments where sediment sizes are coarser (corresponding to steeper beach slopes), the incident wave energy and wave group are correspondingly stronger (Masselink et al., 2007a), which leads to higher wave-induced turbulence (van der Werf et al., 2007). Meanwhile, stronger mean current and flow acceleration are produced by wave breaking on steeper beach slopes. In contrast, infragravity wave may be weaker because of inadequate release of infragravity wave after wave breaking due to limited breaker width (Longuet-Higgins and Stewart, 1964; Symonds et al., 1982; Baldock and Swan, 1996). Hence, we infer that the relative contributions of the TKE, wave group, incident wave, flow acceleration and mean current to SSCs would increase, while that of infragravity wave would decrease correspondingly in the environment with coarser sediment grain size (i.e., steeper beach slope) and vice versa.

Though the relative importance of different hydrodynamics forces has been evaluated by GRA method herebefore, the technique can not quantify the respective contribution of all the relevant factors to SSC (Deng, 1989; Chen and Syu, 2003). Therefore, in order to quantify the contribution of all the relevant factors (hydrodynamic forces and environmental factors) to SSC, further studies were necessary to comprehensively explore the physical mechanism of sediment suspension.

5. Conclusions

A field observation measuring water depth, water surface elevation, high-resolution 3D flow velocity and the near-bed vertical profile of SSCs was conducted throughout the shoaling, breaking and surf bore conditions over a meso-macro tidal beach for nearly three tidal cycles. The aim of this study was to conduct a comprehensive analysis of the tradeoffs among TKE, waves, and SSC in different wave conditions. The main conclusions are as follows:

(1) Variations in relative wave height were a decisive indicator of the differences in TKE intensity among different wave conditions, while the occurrence of the peak TKEs at the wave front within the intrawave cycle was associated with flow acceleration irrespective of wave conditions.
(2) SSCs were well correlated with waves in terms of both incident wave scale and wave group scale which was limited to the shoaling wave condition, while the relationship between the SSC and waves disappeared under the wave breaking and surf bore conditions. The occurrence of near-bed peak SSCs was related to the offshore phase of the incident wave where a wave trough occurred.
(3) The correlated TKE events accounting for 12.2% of the total TKE time records and containing 38.1% of the total turbulent motions were associated with 42.9% of SSC events and 40.0% of total sediment concentrations during the observed time. In addition, it was more effective for TKE to contribute to sediment suspension at the wave group scale than at the incident wave scale, especially under broken wave conditions.
(4) TKE played the most important role in the variations in SSCs among the hydrodynamic factors regardless wave conditions, and flow acceleration played the second most important role under the broken wave condition, while wave group, single wave (including the incident wave and infragravity wave) and advection (mean current) were considered equivalent and less important factors.

Declaration of competing interest

The authors declare that they have no known competing financial interests or personal relationships that could have appeared to influence the work reported in this paper.

Acknowledgments

This study was supported by the National Natural Science Foundation of China (NSFC) (41930537, 41866001, 41666003). The authors thank Zhenpeng Ge and Jinghua Gu for assistance in the field. We are also grateful to Edward Anthony (editor in chief) and two anonymous reviewers for their constructive comments and suggestions that improved the article. All data in this study can access through corresponding author by email.

Appendix A. Supplementary data

Supplementary data to this article can be found online at https://doi.org/10.1016/j.margeo.2020.106190.

References

Aagaard, T., Greenwood, B., 1995. Suspended sediment transport and morphological response on a dissipative beach. Cont. Shelf Res. 15 (9), 1061–1086.
Aagaard, T., Greenwood, B., 2008. Infragravity wave contribution to surf zone sediment transport — the role of advection. Mar. Geol. 251 (1–2), 1–14.
Aagaard, T., Hughes, M.G., 2006. Sediment suspension and turbulence in the swash zone of dissipative beaches. Mar. Geol. 228 (1–4), 117–135.
Aagaard, T., Hughes, M.G., 2010. Breaker turbulence and sediment suspension in the surf zone. Mar. Geol. 271, 250–259.
Aagaard, T., Jensen, S.G., 2013. Sediment concentration and vertical mixing under breaking waves. Mar. Geol. 336, 146–159.
Aagaard, T., Greenwood, B., Hughes, M., 2013. Sediment transport on dissipative, intermediate and reflective beaches. Earth Sci. Rev. 124, 32–50.
Alsina, J.M., Cáceres, I., 2011. Sediment suspension events in the inner surf and swash zone. Measurements in large-scale and high-energy wave conditions. Coast. Eng. 58 (8), 657–670.
Alsina, J.M., Zanden, J.V.D., Cáceres, I., Ribberink, J.S., 2018. The influence of wave groups and wave-swash interactions on sediment transport and bed evolution in the swash zone. Coast. Eng. 140, 23–42.
Austin, M., Masselink, G., O'Hare, T., Russell, P., 2009. Onshore sediment transport on a sandy beach under varied wave conditions: flow velocity skewness, wave asymmetry or bed ventilation? Mar. Geol. 259 (1–4), 86–101.
Balasubramanian, S., Ganapathy, S., 2011. Grey relational analysis to determine optimum process parameters for wire electro discharge machining (WEDM). Int. J. Eng. Sci. 23, 95–101.
Baldock, T.E., Swan, C., 1996. Extreme waves in shallow and intermediate water depths. Coast. Eng. 27, 21–46.
Beach, R.A., Sternberg, R.W., 1996. Suspended-sediment transport in the surf zone: response to breaking waves. Cont. Shelf Res. 16 (15), 0–2003.
Bertin, X., de Bakker, A., van Dongeren, A., Coco, G., André, G., Ardhuin, F., Bonneton, P., Bouchette, F., Castelle, B., Crawford, W.C., Davidson, M., Deen, M., Dodet, G., Guérin, T., Inch, K., Leckler, F., McCall, R., Muller, H., Olabarrieta, M., Roelvink, D., Ruessink, G., Sous, D., Stutzmann, E., Tissier, M., 2018. Infragravity waves: from driving mechanisms to impacts. Earth Sci. Rev. 177, 774–799.
Bolaños, R., Thorne, P.D., Wolf, J., 2012. Comparison of measurements and models of bed stress, bedforms and suspended sediments under combined currents and waves. Coast. Eng. 62 (4), 19–30.
Bonneton, P., Lannes, D., Martins, K., Michallet, H., 2018. A nonlinear weakly dispersive method for recovering the elevation of irrotational surface waves from pressure

measurements. Coast. Eng. 138, 1–8.
Brinkkemper, J.A., Lanckriet, T., Grasso, F., Puleo, J.A., Ruessink, B.G., 2016. Observations of turbulence within the surf and swash zone of a field-scale sandy laboratory beach. Coast. Eng. 113, 62–72.
Brinkkemper, J.A., De Bakker, A.T.M., Ruessink, B.G., 2017. Intrawave sand suspension in the shoaling and surf zone of a field-scale laboratory beach. J. Geophys. Res. Earth Surf. 122 (1), 356–370.
Butt, T., Russell, P., Puleo, J., Miles, J., Masselink, G., 2004. The influence of bore turbulence on sediment transport in the swash and inner surf zones. Cont. Shelf Res. 24, 757–771.
Capo, S., Parisot, J.P., Bujan, S., Senechal, N., 2009. Short time morphodynamics response of the Truc Vert beach to storm conditions. J. Coast. Res. 56 (2), 1741–1745.
Chen, M.Y., Syu, M.J., 2003. Film analysis of activated sludge microbial discs by the Taguchi method and grey relational analysis. Bioprocess Biosyst. Eng. 26 (2), 83–92.
Chou, J.R., Tsai, H.C., 2009. On-line learning performance and computer anxiety measure for unemployed adult novices using a grey relation entropy method. Inform. Process. Manag. 45 (2), 200–215.
Christensen, D.F., Brinkkemper, J., Ruessink, G., Aagaard, T., 2019. Field observations of turbulence in the intertidal and shallow subtidal zones. Cont. Shelf Res. 170, 21–32.
Conley, D.C., Beach, R.A., 2003. Cross-shore sediment transport partitioning in the nearshore during a storm event. J. Geophys. Res. Oceans 108 (C3), 103–133.
Cox, D.T., Kobayashi, N., 2000. Identification of intense, intermittent coherent motions under shoaling and breaking waves. J. Geophy. Res. Oceans 105 (C6).
Dai, Z.J., Liu, J.T., Lei, Y.P., Zhang, X.L., 2010. Patterns of sediment transport pathways on a headland bay beach-Nanwan beach, South China: a case study. J. Coastal Res. 26 (6), 1096–1103.
Dally, W.R., Dean, R.G., 1984. Suspended sediment transport and beach profile evolution. J. Waterw. Port Coast. 110, 15–33.
De Bakker, A.T.M., Brinkkemper, J.A., Van, d.S.F., Tissier, M.F.S., Ruessink, B.G.., 2016. Cross-shore sand transport by infragravity waves as a function of beach steepness. J. Geophys. Res. Earth Surf. 121 (10), 1786–1799.
Deng, J.L., 1989. Introduction to Grey system theory. J. Grey Syst. 1, 1–24.
Dong, G.H., Ma, Y.X., Ma, X.Z., 2008. Cross-shore variations of wave groupiness by wavelet transform. Ocean Eng. 35 (7), 676–684.
Drake, T.G., Calantoni, J., 2001. Discrete particle model for sheet flow sediment transport in the nearshore. J. Geophy. Res. 106 (C9), 19859.
Elgar, S., 1987. Relationships involving third moments and bispectra of a harmonic process. IEEE Trans. Acoust. Speech Signal Process. 35 (12), 1725–1726.
Fagherazzi, S., Mariotti, G., Porter, J.H., McGlathery, K.J., Wiberg, P.L., 2010. Wave energy asymmetry in shallow bays. Geophys. Res. Lett. 2010, 37.
Foster, D.L., Holman, R.A., Beach, R.A., 1994. Correlation between sediment suspension events and shear instabilities in the bottom boundary layer of the surf zone. In: Arcilla, A.S., Stive, M.J.F., Kraus, N.C. (Eds.), Coastal Dynamics'94. Am. Soc. of Civ. Eng, New York, pp. 712–726.
Foster, D.L., Beach, R.A., Holman, R.A., 2006. Turbulence observations of the nearshore wave bottom boundary layer. J. Geophys. Res. Oceans 111, C04011.
Ge, Z.P., Dai, Z.J., Pang, W.H., Li, S.S., Wei, W., Mei, X.F., Hu, H., Gu, J.H., 2017. Lidar-based detection of the post-typhoon recovery of a meso-macro-tidal beach in the Beibu Gulf, China. Mar. Geol. 391, 127–143.
Gibbons, D.T., Jones, G., Siegel, E., Hay, A., Johnson, F., 2005. Performance of a new submersible Tide-Wave recorder, Oceans. In: Proceedings of MTS/IEEE. vol. 2. IEEE, New York, pp. 1057–1060.
Gonzalez-Rodriguez, D., Madsen, O.S., 2007. Seabed shear stress and bedload transport due to asymmetric and skewed waves. Coast. Eng. 54 (12), 914–929.
Grasmeijer, B.T., Kleinhans, M.G., 2004. Observed and predicted bed forms and their effect on suspended sand concentrations. Coast. Eng. 51 (5–6), 351–371.
Grasso, F., Ruessink, B.G., 2011. Vertical structure of turbulence dissipation rate in the shallow-water surf zone. J. Coast. Res. SI 64, 90–94.
Grasso, F., Castelle, B., Ruessink, B.G., 2012. Turbulence dissipation under breaking waves and bores in a natural surf zone. Cont. Shelf Res. 43, 133–141.
Hanes, D.M., Huntley, D.A., 1986. Continuous measurements of suspended sand concentration in a wave dominated nearshore environment. Cont. Shelf Res. 6, 585–596.
Hansen, J.B., Svendsen, I.A., 1984. A theorethical and experimental study of the undertow. In: Proc. 19th Intl. Conf. on Coast. Eng. ASCE, pp. 2246–2262.
Heathershaw, A., 1974. Bursting phenomena in the sea. Nature 248, 394–395.
Hu, P., Han, J.J., Li, W., Sun, Z.L., He, Z.G., 2018. Numerical investigation of a sandbar formation and evolution in a tide-dominated estuary using a hydro-sediment-morphodynamic model. Coast. Eng. J. 60 (4), 466–483.
Hu, Z., Wang, Z.B., Zitman, T.J., Stive, M.J.F., Bouma, T.J., 2015. Predicting long-term and short-term tidal flat morphodynamics using a dynamic equilibrium theory. J. Geophys. Res. Earth Surf. 120 (9), 1803–1823.
Huang, H., Dai, Z.J., Shi, W.Y., Sheng, K., 2011. Deposition characteristics of beach profile in strong-tidal environment – a case study of Yintan, Guangxi during spring. Journal of Tropical Oceanography 30 (4), 71–76.
Huang, Y.P., Huang, C.C., 1996. The integration and application of fuzzy and grey modeling methods. Fuzzy Sets Syst. 78, 107–119.
Inman, D.L., Bowen, A.J., 1963. Flume experiments on sand transport by waves and currents. In: Am. Soc. Civil Engr. Proc. 8th Conf. Coastal Engnr, pp. 137–150.
Jaffe, B.E., Rubin, D.M., 1996. Using nonlinear forecasting to learn the magnitude and phasing of time-varying sediment suspension in the surf zone. J. Geophy. Res. Atmos. 101 (C6), 14283–14296.
Jaffe, B.E., Sallenger, A.H., 1992. The contribution of suspension events to sediment transport in the surf zone. In: Proceedings of the International Conference on Coastal Engineering. ASCE, pp. 2680–2693.
Jaffe, B.E., Sternberg, R.W., Sallenger, A.H., 1984. The role of suspended sediment in shore-normal beach profile changes. In: Proceedings Coastal Engineering Conference. ASCE press, Houston, Texas, pp. 1983–1996.
Kadier, A., Abdeshahian, P., Simayi, Y., Ismail, M., Hamid, A.A., Kalil, M.S., 2015. Grey relational analysis for comparative assessment of different cathode materials in microbial electrolysis cells. Energy 90, S0360544215008646.
Kassem, H., Thompson, C.E.L., Amos, C.L., Townend, I.H., 2015. Wave-induced coherent turbulence structures and sediment resuspension in the nearshore of a prototype-scale sandy barrier beach. Cont. Shelf Res. 109, 78–94.
Kobayashi, N., Payo, A., Schmied, L., 2008. Cross-shore suspended sand and bedload transport on beaches. J. Geophy. Res. Oceans 113 (C7).
Kularatne, S., Pattiaratchi, C., 2008. Turbulent kinetic energy and sediment resuspension due to wave groups. Cont. Shelf Res. 28 (6), 0–736.
Leclaire, P.D., Ting, F.C.K., 2017. Measurements of suspended sediment transport and turbulent coherent structures induced by breaking waves using two-phase volumetric three-component velocimetry. Coast. Eng. 121, 56–76.
Lee, J., O'Neil, S., Bedford, K., Van Evra, R., 1994. A Bottom Boundary Layer Sediment Response to Wave Groups. Chapter 131, Coast. Eng. 1994. ASCE, pp. 1827–1836.
Leonardi, N., Ganju, N.K., Fagherazzi, S., 2015. A linear relationship between wave power and erosion determines salt-marsh resilience to violent storms and hurricanes. P. Natl. Acad. Sci. USA 113 (1), 64.
List, J.H., 1991. Wave groupiness variations in the nearshore. Coast. Eng. 15, 475–496.
Longo, S., Petti, M., Losada, I.J., 2002. Turbulence in the swash and surf zones: a review. Coast. Eng. 45 (3), 129–147.
Longuet-Higgins, M.S., 1984. Statistical properties of wave groups in a random sea state. Philos. Trans. R. Soc. Lond. 312 (1521), 219–250.
Longuet-Higgins, M.S., Stewart, R.W., 1964. Radiation stresses in water waves; a physical discussion, with applications. Deep-Sea Research and Oceanographic Abstracts 11 (4), 529–562.
Masselink, G., Auger, N., Russell, P., O'Hare, T., 2007a. Short-term morphological change and sediment dynamics in the intertidal zone of a macrotidal beach. Sedimentology 54 (1), 39–53.
Masselink, G., Austin, M.J., O'Hare, T.J., Russell, P.E., 2007b. Geometry and dynamics of wave ripples in the nearshore zone of a coarse sandy beach. J. Geophy. Res. Oceans 112 (C10022).
Miles, J., Thorpe, A., 2015. Bedform contributions to cross-shore sediment transport on a dissipative beach. Coast. Eng. 98, 65–77.
Murray, R.B.O., Thorne, P.D., Hodgson, D.M., 2011. Intrawave observations of sediment entrainment processes above sand ripples under irregular waves. J. Geophy. Res. Oceans 116 (C1).
Murray, R.B.O., Hodgson, D.M., Thorne, P.D., 2012. Wave groups and sediment resuspension processes over evolving sandy bedforms. Cont. Shelf Res. 46 (none).
Nadaoka, K., Hino, M., Koyano, Y., 1989. Structure of the turbulent flow field under breaking waves in the surf zone. J. Fluid Mech. 204, 359–387.
Nakato, T., Locher, F.A., Glover, J.R., Kennedy, J.F., 1977. Wave entrainment of sediment from rippled beds. Pro. Asce Ww. 103 (1), 83–99.
Nichols, C.S., Foster, D.L., 2007. Full-scale observations of wave-induced vortex generation over a rippled bed. J. Geophys. Res. Oceans 112, C10015.
Nielsen, P., 2006. Sheet flow sediment transport under waves with acceleration skewness and boundary layer streaming. Coast. Eng. 53, 749–758.
Nielsen, P., van der Wal, K., Gillan, L., 2002. Vertical fluxes of sediment in oscillatory sheet flow. Coast. Eng. 45, 61–68.
O'Donoghue, T., Wright, S., 2004. Flow tunnel measurements of velocities and sand flux in oscillatory sheet flow for well-sorted and graded sands. Coast. Eng. 51 (11 − 12), 1163–1184.
Osborne, P.D., Greenwood, B., 1992. Frequency dependent cross-shore suspended sediment transport. 1. A non-barred shoreface. Mar. Geol. 106 (1–2), 1–24.
Osborne, P.D., Greenwood, B., 1993. Sediment suspension under waves and currents: time scales and vertical structure. Sedimentology 40 (4), 599–622.
Pang, W.H., Dai, Z.J., Ge, Z.P., Li, S.S., Mei, X.F., Gu, J.H., Huang, H., 2019. Near-bed cross-shore suspended sediment transport over a meso-macro tidal beach under varied wave conditions. Estuar. Coast. Shelf S. 217, 69–80.
Puleo, J.A., Holland, K.T., Plant, N.G., Slinn, D.N., Hanes, D.M., 2003. Fluid acceleration effects on suspended sediment transport in the swash zone. J. Geophy. Res. Oceans 108 (C11), 3350.
Raubenheimer, B., Guza, R.T., Elgar, S., 1996. Wave transformation across the inner surf zone. J. Geophys. Res. 101 (C11), 25589.
Ribberink, J.S., Al-Salem, A.A., 1995. Sheet flow and suspension of sand in oscillatory boundary layers. Coast. Eng. 25 (3–4), 205–225.
Roelvink, J.A., Stive, M.J.F., 1989. Bar-generating cross-shore flow mechanisms on a beach. J. Geophys. Res. Atmos. 94 (C4), 4785–4800.
Ruessink, B.G., 2010. Observation of turbulence within a natural surf zone. J. Phys. Oceanogr. 40, 2696–2712.
Ruessink, B.G., Michallet, H., Abreu, T., Sancho, F., Van der A, D.A., Van der Werf, J.J., Silva, P.A., 2011. Observations of velocities, sand concentrations, and fluxes under velocity-asymmetric oscillatory flows. J. Geophys. Res. Oceans 116, C03004.
Scott, N.V., Hsu, T.J., Cox, D., 2009. Steep wave, turbulence, and sediment concentration statistics beneath a breaking wave field and their implications for sediment transport. Cont. Shelf Res. 29 (20), 0–2317.
Smyth, C., Hay, A.E., 2003. Near bed turbulence and bottom friction during SandyDuck97. J. Geophy. Res. Oceans 108 (C6), 3197.
Soulsby, R.L., Humphery, J.D., 1990. Field observations of wave-current interaction at the sea bed. Water Wave Kinematics 413–428.
Splinter, K.D., Holman, R.A., Plant, N.G., 2011. A behavior-oriented dynamic model for sandbar migration and 2DH evolution. J. Geophys. Res. Oceans 116, C01020.
Stansby, P.K., Feng, T., 2005. Kinematics and depth-integrated terms in surf zone waves from laboratory measurements. J. Fluid Mech. 529, 279–310.
Stapleton, K.R., Huntley, D.A., 1995. Seabed stress determinations using the inertial

dissipation method and the turbulent kinetic energy method. Earth Surf. Proc. Land. 20 (9), 807–815.
Sternberg, R.W., Shi, N.C., Downing, J.P., 1985. Field investigations of suspended sediment transport in the nearshore zone. In: Proceedings 19th Coastal Engineering Conference. American Society of Civil Engineers, New York, pp. 1782–1798.
Svendsen, I.A., 1987. Analysis of surf zone turbulence. J. Geophys. Res. Oceans 92, 5115–5124.
Symonds, G., Huntley, D., Bowen, A.J., 1982. Two-dimensional surf beat: Long wave generation by a time-varying breakpoint. J. Geophy. Res. 87, 492–498.
Tang, Y.S., Ma, S.C., Chung, L.K., 1995. Determination of optimal cutting parameters in wire electrical discharge machining. Int J Mach Tool Manu 35 (12), 1693–1701.
Ting, F.C.K., 2002. Laboratory study of wave and turbulence characteristics in narrow-band irregular breaking waves. Coast. Eng. 46 (4), 291–313.
van der Werf, J.J., Doucette, J.S., O'Donoghue, T., Ribberink, J.S., 2007. Detailed measurements of velocities and suspended sand concentrations over full-scale ripples in regular oscillatory flow. J. Geophys. Res. Earth Surf. 112, F02012.
Veltcheva, A., Soares, C.G., 2016. Analysis of wave groups by wave envelope-phase and the Hilbert Huang transform methods. Appl. Ocean Res. 60, 176–184.
Villard, P.V., Osborne, P.D., 2002. Visualization of wave-induced suspension patterns over two-dimensional bed forms. Sedimentology 49, 363–378.
Villard, P.V., Osborne, P.D., Vincent, C.E., 2000. Influence of wave groups on SSC patterns over vortex ripples. Cont. Shelf Res. 20, 2391–2410.
Vincent, C.E., Hanes, D.M., 2002. The accumulation and decay of nearbed suspended sand concentration due to waves and wave groups. Cont. Shelf Res. 22, 1987–2000.
Vincent, C.E., Hanes, D.M., Bowen, A.J., 1991. Acoustic measurements of suspended sand on the shoreface and the control of concentration by bed roughness. Mar. Geol. 96 (1–2), 1–18.
Williams, J.J., Rose, C.P., Thorne, P.D., 2002. Role of wave groups in resuspension of sandy sediments. Mar. Geol. 183 (1), 17–29.
Wong, H., Hu, B.Q., Ip, W.C., Xia, J., 2006. Change-point analysis of hydrological time series using grey relational method. J. Hydrol. 324, 323–338.
Xu, G., Yang, Y.P., Lu, S.Y., Li, L., Song, X., 2011b. Comprehensive evaluation of coal-fired power plants based on grey relational analysis and analytic hierarchy process. Energ Policy 39 (5), 2343–2351.
Xu, J., Sheng, G.P., Luo, H.W., Fang, F., Li, W.W., Zeng, R.J., Tong, Z.H., Yu, H.Q., 2011a. Evaluating the influence of process parameters on soluble microbial products formation using response surface methodology coupled with grey relational analysis. Water Res. 45 (2), 674–680.
Yoon, H.D., Cox, D.T., 2012. Cross-shore variation of intermittent sediment suspension and turbulence induced by depth-limited wave breaking. Cont. Shelf Res. 47, 93–106.
Yu, Y., Sternberg, R.W., Beach, R.A., 1993. Kinematics of breaking waves and associated suspended sediment in the nearshore zone. Cont. Shelf Res. 13 (11), 1219–1242.
Zhou, G., Huang, J., Yue, T., Luo, Q., Zhang, G., 2015. Temporal-spatial distribution of wave energy: a case study of Beibu Gulf, China. Renew. Energ. 74, 344–356.